(La Mona South)

In the field, III-stage dacite (Tdc₃) whose color changed to white were found here and there and regarded as the signs of hydrothermal alteration, but as a result of X-ray diffractometrical study, no formation of clay minerals was found. Accordingly, the influene of hydrothermal alteration on this dacite is judged to be small even if it exists. However, comparatively a high percentage of K-feldspar is contained in each sample and this K-feldspar is highly possible to be a K-feldspar which has the form of adularia formed by diagenesis pointed out by Honda & Matsueda (1979) rather than primary K-feldspar when judged from the field occurrence (rock color changing to white). From the viewpoint of hydrothermal alteration, relationship with Kuroko type deposits cannot be expected.

Other: In Canada area in the northern part of the survey area, a weak alteration zone, which is not subject to fractures clearly, were found in IV-stage andesites (Tad₄). The X-ray diffractometrical study of this zone showed that clay minerals were not formed, but quartz and K-feldspar were formed while the plagioclase of the original rock remained. As the combination of quartz and K-feldspar is found frequently in gold (silver) deposits, future study is required from this point of view.

3-5-4　On Residual Content of Plagioclase

The residual content of plagioclase, the mineral which is decomposed most easily by hydrothermal alteration, was investigated. The place where the residual plagioclase can be noticed by X-ray diffractometrical study corresponds to the III-zone in the alteration zoning. Around the residual zone, plagioclase has been decomposed completely as shown in Fig. 3-13 in contrast with the distribution shown in Fig. 3-11. However, at the NE-SW end of the hanging wall dacite (Kdc₂), plagioclase begins to remain again and alteration tends to decline. In addition, several isolated residual zones are distributed in the eastern part of the La America deposit.

The La America deposit is located between perfect decomposition zone and residual zone, but the Descubridora deposit is in a residual zone of plagioclase. As pointed out in the section of alteration zoning, the fact that the zones of high alteration degrees seem to exist rather in other places than known deposits requires attention in Kuroko exploration.
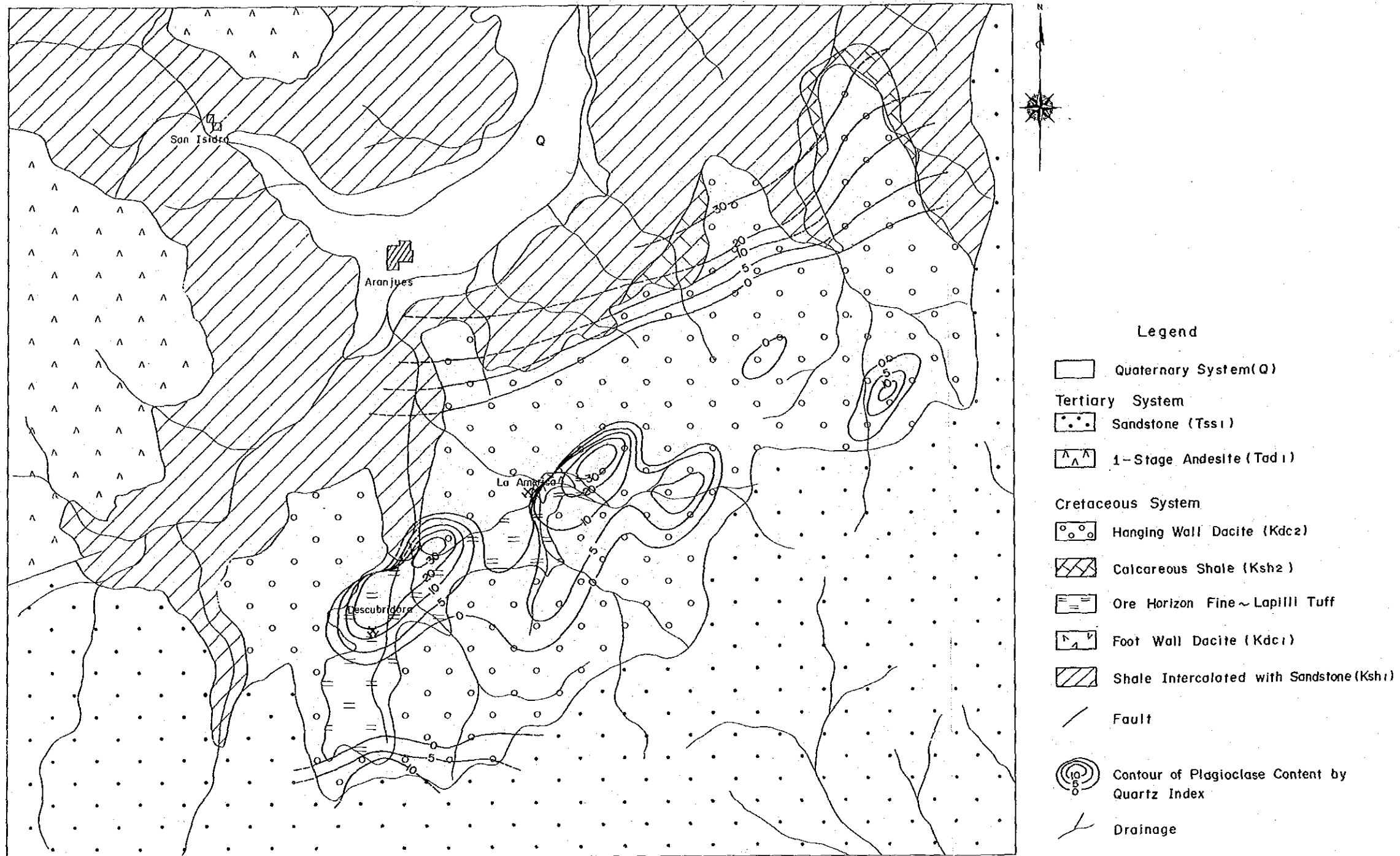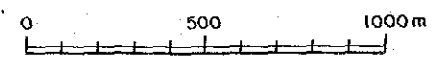
Legend

Quaternary System (Q)

Tertiary System
- Sandstone (Tss1)
- 1-Stage Andesite (Tad1)

Cretaceous System
- Hanging Wall Dacite (Kdc2)
- Calcareous Shale (Ksh2)
- Ore Horizon Fine ~ Lapilli Tuff
- Foot Wall Dacite (Kdc1)
- Shale Intercalated with Sandstone (Ksh1)

Fault

Contour of Plagioclase Content by Quartz Index

Drainage

Fig. 3-13 Distribution of Plagioclase Content in La America - Descubridora Area

0   500   1000 m

3-5-5   On Chlorite

Chlorite is comparatively a popular mineral in Kuroko type deposits, and its appearance frequency is high also in this area. About the chemical composition of chlorite which appears in the altered zone around a Kuroko type deposit, it has been known that the chemical composition of chlorite near the deposit differs from that in the peripheral part (Izawa et al., 1978; Urabe & Scott, 1982-A). Chlorite shows the 001 reflection from the first order to the fifth order depending upon the basal distance of about 14 $\overset{\circ}{A}$ in X-ray diffractometry, and the relative intensity of these basal reflections varies with the chemical compositions of chlorite. In this survey, octahedron cation composition and heavy atom (Fe) distribution were determined from the intensity ratios of three reflection values on a triangular figure of I (14 $\overset{\circ}{A}$) – I (7 $\overset{\circ}{A}$) – I (4.7 $\overset{\circ}{A}$) devised by Oinuma et al. (1972). (Fig. 3-14)

If the chemical composition of chlorite is assumed as $(Mg, Al)_6 - yFey (Si, Al)_4 O_{10}(OH)_8$, the y of chlorite in this survey area changes in a range of Y = 1.5 - 3.5. The pyroclastics of ore horizon which are distributed near the isoplethic line y = 2 are all those collected in the Descubridora tunnel, and those of y = 2.5 - 3 were collected in the La America tunnel. In spite of their position near the deposit, they are chlorites richer in iron than the former. This fact does not agree with the general phenomenon that chlorite richer in magnesium is formed near ore deposit in a Kuroko type deposit, and the reason for this disagreement is unclear. It may be a feature of the La America deposit or the result of chlorite composition change caused by the overlapping of the subsequent Coucha type vein mineralization.

The chemical compositions of chlorite in the hanging wall dacite (Kdc$_2$) include that plotted in a range of y = 2 - 2.5 and that with a value near y = 3.5. The former chlorite is similar to that in the pyroclastics (Koh) of ore horizon in La America-Descubridora in relation to composition, but the latter chlorite is that richer in iron. As a reason for this difference, the influence of the position of collecting the latter sample, which was near granophyre by chance, can be considered, but the number of examples was too small to clarify the reason adequately. The two chlorite samples in the host rock of the Plomosas vein have almost the same composition and are richer in iron than the samples related with Kuroko type deposits, and this agrees with the general tendency known till today.

Fig. 3-14 shows the change of the composition of chlorite in the footwall dacite of Fukazawa deposit, which is a representative Cenozoic Kuroko deposit in Japan, with the distance from the deposit. Although there is local disturbance of about 0.5 in the value of y in the changing tendency of y, a tendency that y decreases (decrease in iron and increase in magnesium) with approach to the deposit can be noticed. Therefore, it is useful for estimating a distance from a deposit.

Chlorite in this area has chemical compositions almost equivalent to those of chlorite appearing in places 0.7 - 4 km apart from the deposit around Fukazawa deposit, but chlorite like that, which is produced in Fukazawa deposit and is extremely rich in magnesium to an extent of y = 0.5, has not been found. These characteristics of chlorite can be interpreted that the chlorite in this survey area is different from that of the Kuroko deposit and relatively richer in iron, or that, as pointed out in the section of alteration zoning mentioned before, the center of alteration may be concealed in other places than known Kuroko type deposits.
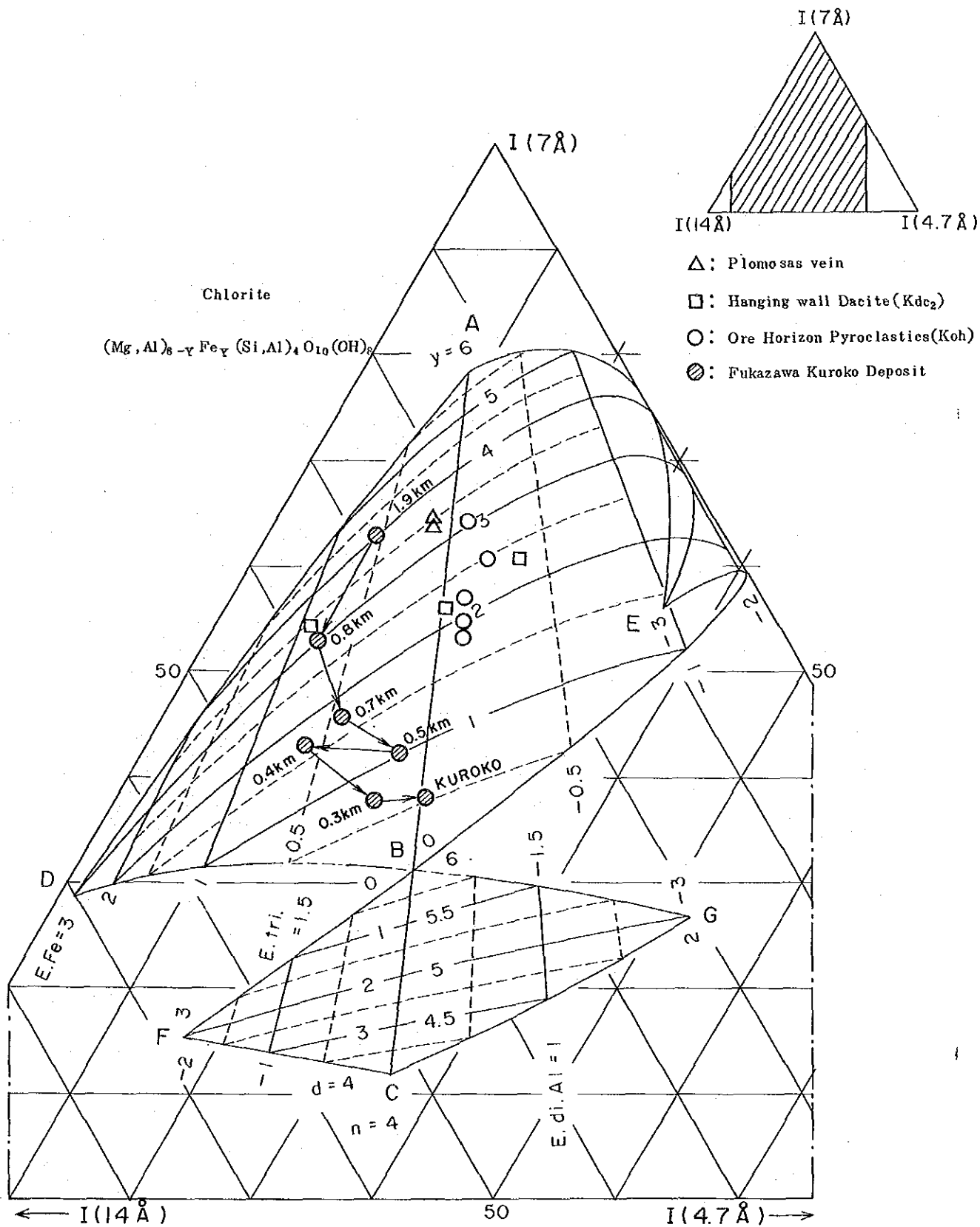
Fig.3-14 Diagram on Chemical Composition of Chlorite

CHAPTER 4   GEOCHEMICAL EXPLORATION

CHAPTER 4 GEOCHEMICAL EXPLORATION

4-1 Geochemical Exploration using Stream Sediments

4-1-1 Method of Survey

(1) Sample Collection

In the geochemical exploration using stream sediments, samples were collected checking sample collecting points, which were established previously so as to cover the entire survey area, on topographical maps and with barometers. In a survey area of 1,000 km^2, 1,505 samples were collected. Sample collecting places were on the bank of a stream, the sandbank in a stream or in the underneath of a rock, etc., and a sample of about 30 g of -80 mesh size was collected in each place. The analytical results of these samples are shown in Apx. 1 together with the geology which determines the origin of each sample, collected position, etc.

(2) Preparation of Sample and Detection Limit of Analysis

The samples were dried at the survey base (Talpa de Allende), magnetite was removed from them with magnets, about a quantity of 20 g was separated from each sample for analysis, and after preparing sample lists, the samples for analysis were sent to Hanaoka Laboratory of Dowa Mining Co., Ltd.

Analytical detection limits were all 0.1 ppm for Ag, Cu, Pb and Zn. As the frequency of appearance of values below the detection limit was high (66%) for Ag, statistical treatment was carried out by assuming the values below the detection limit as 0.01 ppm.

4-1-2 Statistical Treatment of Analytical Values

Single variable and multivariable analyses were carried out for the four elements (Ag, Cu, Pb and Zn) of 1,505 samples collected during this survey. In geochemical data analyses, it has been known empirically that the frequency distribution of the contents of minor elements contained in geochemical samples assumes log normal distribution (Lepeltier, 1969). Accordingly, it has been the general method of determining anomalous values to pay attention to the deviation (anomalous population) from the log normal distribution (background population) shown by the most part of a certain indicator. The population handled in geochemical exploration is usually the composite population of the background population and the anomalous population, and it becomes an important subject how to divide these two in conformity with actual conditions. Apart from the case where the object composite population assumes log normal distribution, when the population assumes a distribution deviated from the log normal distribution, particular consideration is required. In the past, a method to determine background values and threshold values using a cumulative frequency distribution curve by Lepeltier (1969) and Sinclair (1976) has been used as a method to solve this problem.

However, a composite population shown by actual geochemical data is usually an assembly of several kinds of populations each having different geochemical

characteristics. Therefore, there is a problem in the manner to divide a composite population into each element population at the bending points on the cumulative frequency distribution curve or at the middle points of curves which appear near the boundaries of plural different populations. As we thought is rational to use the method to determine a frequency curve by determining a spline function approximate to the cumulative frequency curve and its derivative of the first order, which was recently devised by Otsu et al. (1983), to solve the above problem, we used this method for determining the threshold values of single variables. However, to a case where the cumulative frequency curve or histogram agrees well with the log normal distribution curve, the meaning to apply the method by Otsu et al. becomes less, because the population in this case is regarded to be composed of a single population. However, in this survey, it was possible to detect some abnormal population for each of the four elements.

4-1-3 Background Geology and Indicator Content

The contents of indicators in the stream sediments depend upon the geological conditions and the degrees of mineralization and alteration of the background area from which the sediments came from. Accordingly, geochemical characteristics for respective geological units are shown in Table 4-1. However, as the number of samples included in each geological unit was small, threshold values were not determined. According to this table, geological units which have background areas with clearly higher geometric means than that of the entire area are as follows.

Ag : I-stage dacites (Tdc_1)

Cu : I-stage andesites (Tad_1)

Pb : the same through all the geological units

Zn : Cretaceous system

Geological units whose distribution characteristics of indicator contents show positive skewness are extracted as follows for reference.

Ag : (distribution characteristics unclear)

Cu : (none)

Pb : Cretaceous system, sandstone (Tss_1), II-stage andesites (Tad_2)

Zn : Cretaceous system, I-stage andesites (Tad_1), sandstone (Tss_1), II-stage andesites (Tad_2)

4-1-4 Determination of Threshold Values

Threshold values were determined by smoothing a cumulative frequency curve, drawing a frequency distribution curve, which was determined from the differential coefficients of the smoothed curve, using a spline function, and extracting high content peaks for principal peaks.

Table 4-1　Statistical Parameters of Geochemical Indicators

Rock code	Number of Sample	Geometric Mean (ppm)				Threshold (ppm)				Minimum Value (ppm)				Maximum Value (ppm)				Geometric Standard Deviation				Distribution Type			
		Ag	Cu	Pb	Zn	Ag	Cu	Pb	Zn	Ag	Cu	Pb	Zn	Ag	Cu	Pb	Zn	Ag	Cu	Pb	Zn	Ag	Cu	Pb	Zn
Whole Rocks	1505	0.03	12.9	52.4	74.3	0.54	130	114	356	0.01	0.10	11.0	21.4	8.10	477.7	410.2	3,345.0	0.63	0.52	0.11	0.20	-	N-N	N-P	N-P
1 Cretaceos System	124	0.03	28.0	58.5	116.1	-	-	-	-	0.01	0.10	27.4	39.6	8.10	477.7	410.2	3,345.0	0.76	0.61	0.15	0.36	-	N-N	N-P	N-P
2 I-Stage Andesites(Tad 1)	153	0.014	47.6	54.9	72.3	-	-	-	-	0.01	0.60	23.8	26.0	0.70	231.5	117.9	264.1	0.44	0.29	0.08	0.17	-	N-N	N-O	N-P
3 Sandstone(Tss 1)	105	0.018	19.9	53.9	71.7	-	-	-	-	0.01	1.90	32.2	28.3	0.30	65.1	161.0	525.5	0.49	0.29	0.08	0.16	-	N-N	N-P	N-P
4 II-Stage Andesites(Tad 2)	251	0.021	12.0	51.6	74.9	-	-	-	-	0.01	0.10	24.8	31.8	0.50	99.9	139.4	315.8	0.54	0.41	0.12	0.15	-	N-O	N-P	N-P
5 III-, IV-Stage Andesites (Tad 3, Tad 4)	487	0.032	8.4	51.1	73.0	-	-	-	-	0.01	0.10	11.0	24.2	1.90	101.6	149.8	258.4	0.64	0.49	0.11	0.16	-	N-O	N-O	N-O
6 I-Stage Dacites(Tad 1)	85	0.077	6.4	51.7	66.3	-	-	-	-	0.01	0.10	33.5	31.0	0.35	46.7	77.5	182.9	0.64	0.48	0.08	0.15	-	N-O	N-O	N-O
7 Intrusives(Gd, Adm, Gph)	134	0.017	9.7	51.9	63.2	-	-	-	-	0.01	0.10	16.3	21.4	0.70	138.0	102.5	391.0	0.49	0.46	0.12	0.19	-	N-O	N-O	N-O
8 Others(Tsb 1, etc.)	166	0.061	12.1	50.6	69.9	-	-	-	-	0.01	0.10	27.0	22.4	2.50	77.9	86.4	189.1	0.67	0.47	0.09	0.18	-	N-N	N-O	N-O

Abbreviation

N-O : Log normal distribution without skewness
N-P : Log normal distribution with positive skewness
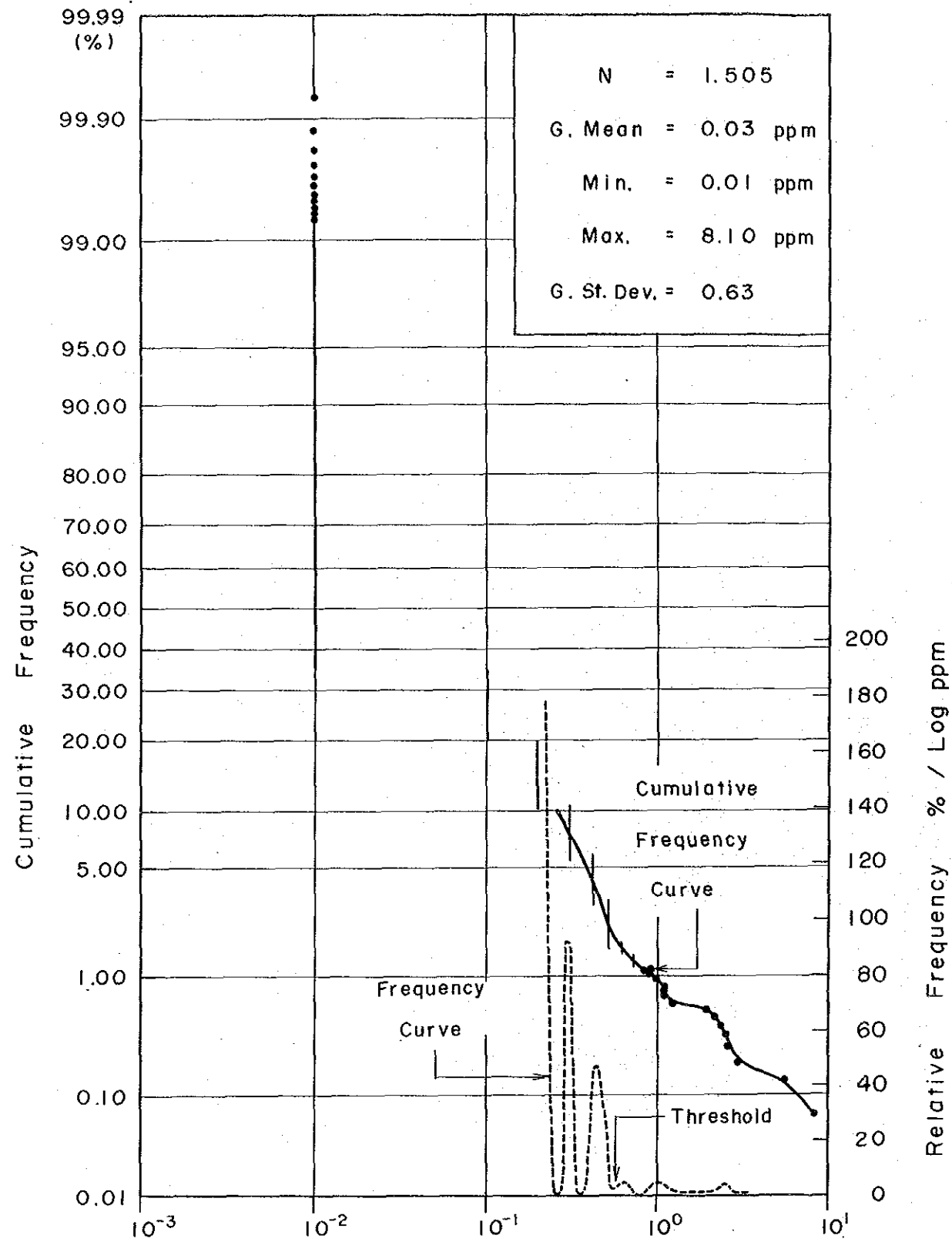N-N : Log normal distribution with negative skewness

Fig. 4-1   Frequency and Cumulative
Frequency Curve (Ag)
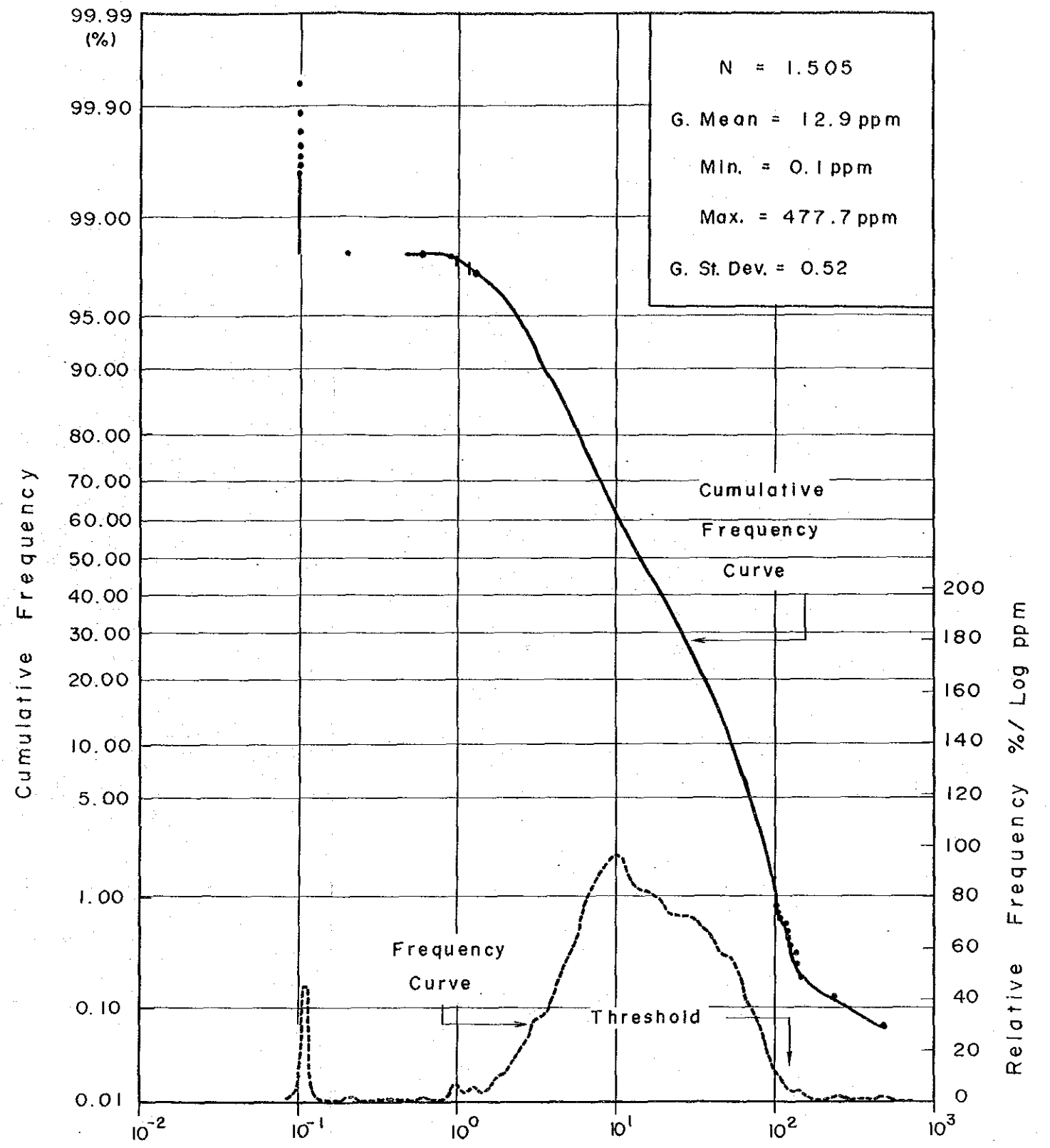

Fig. 4-2   Frequency and Cumulative
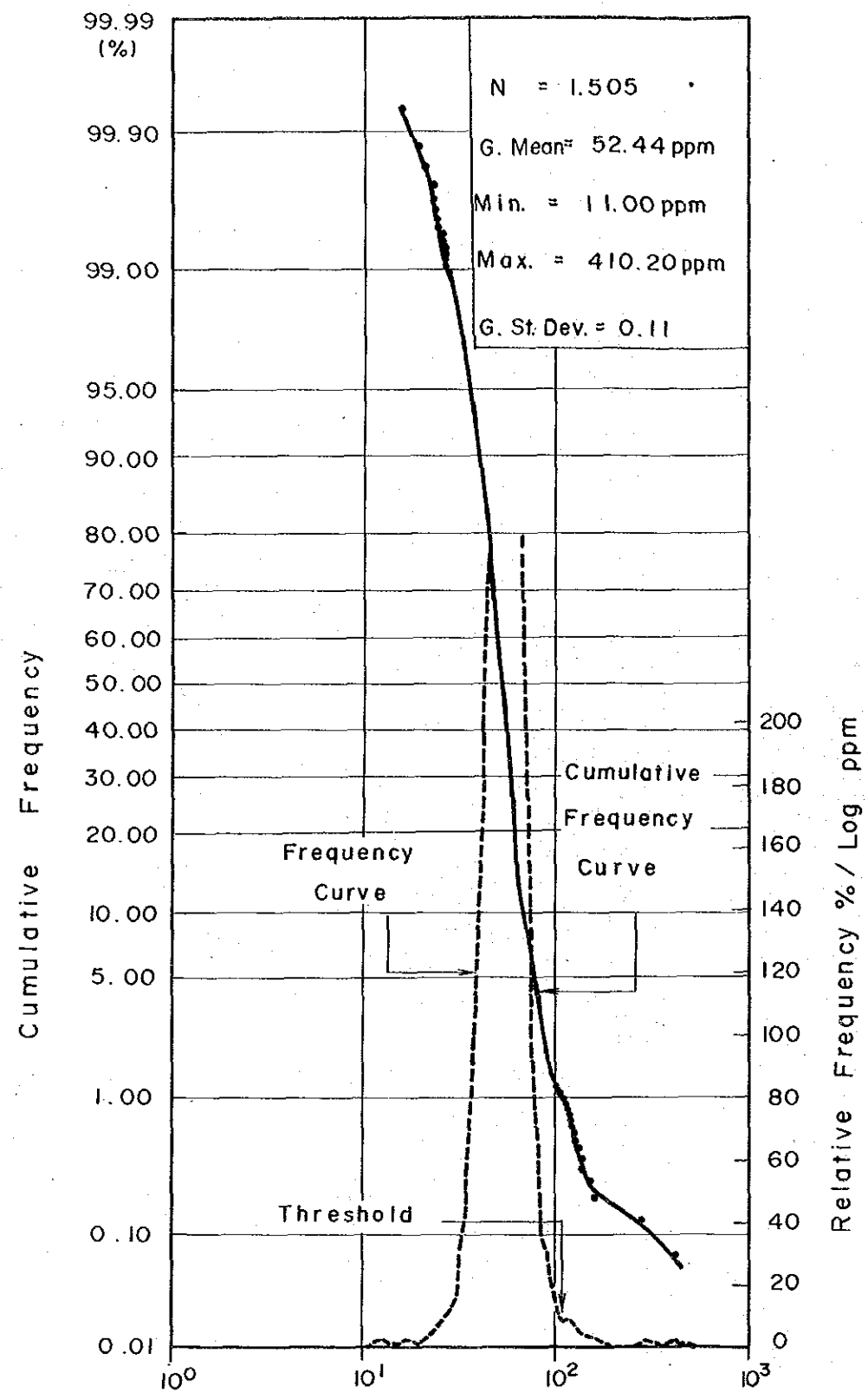Frequency Curve (Cu)

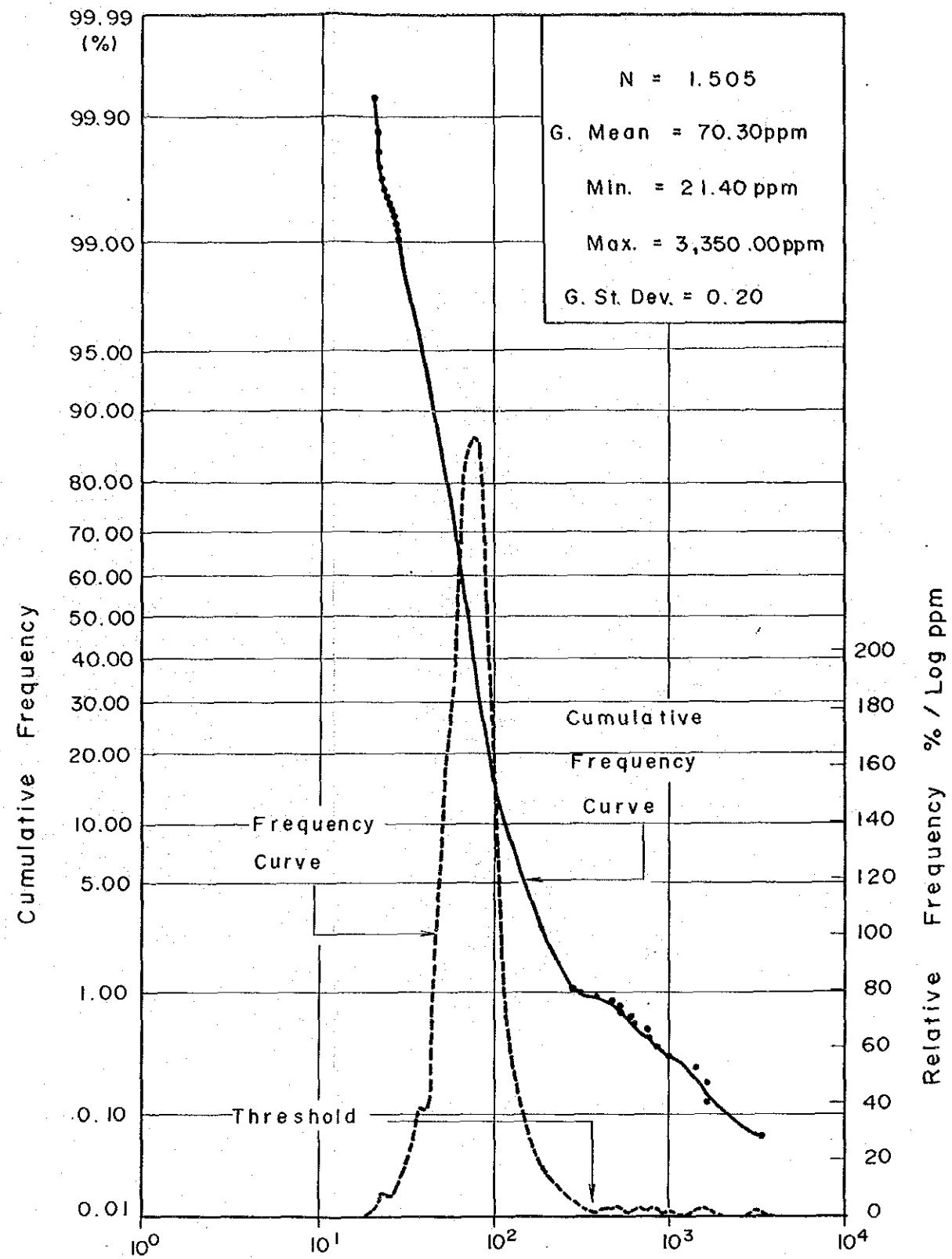Fig. 4-3   Frequency and Cumulative Frequency Curve (Pb)

Fig. 4-4   Frequency and Cumulative Frequency Curve (Zn)
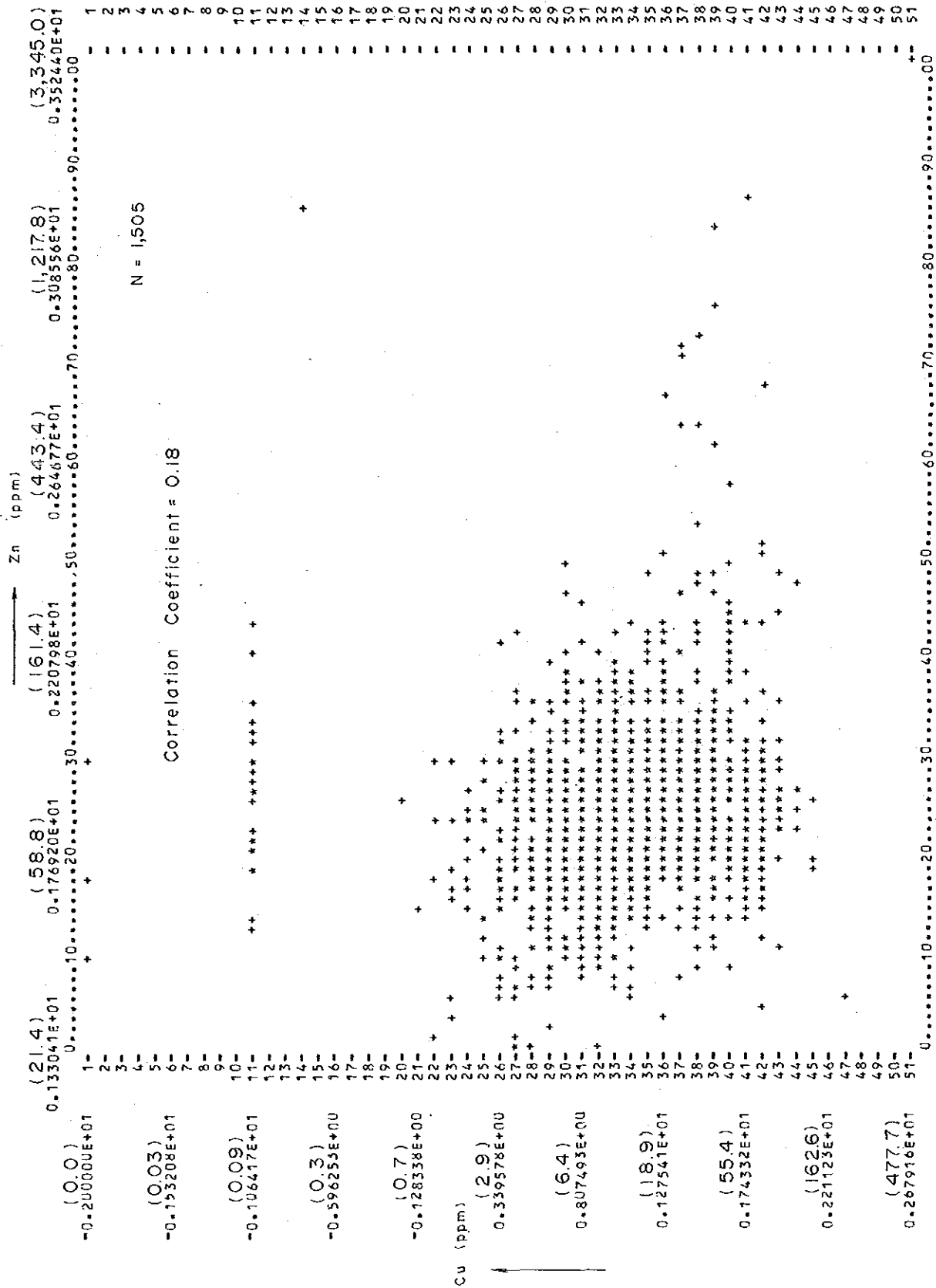
Fig.4-5 Scatter Diagram of All Rock Facies (Cu -Zn)

Zn (ppm)

Correlation Coefficient = 0.55

N = 1,505

Pb (ppm)

Fig.4-6 Scatter Diagram of All Rock Facies (Pb-Zn)

---- LOGARIHTM ----

Zn (ppm)

Pb (ppm)

N = 124

Correlation Coefficient = 0.842

Zn (ppm)

Pb (ppm)

Fig.4-7 Scatter Diagram of Cretaceous System(Pb-Zn)

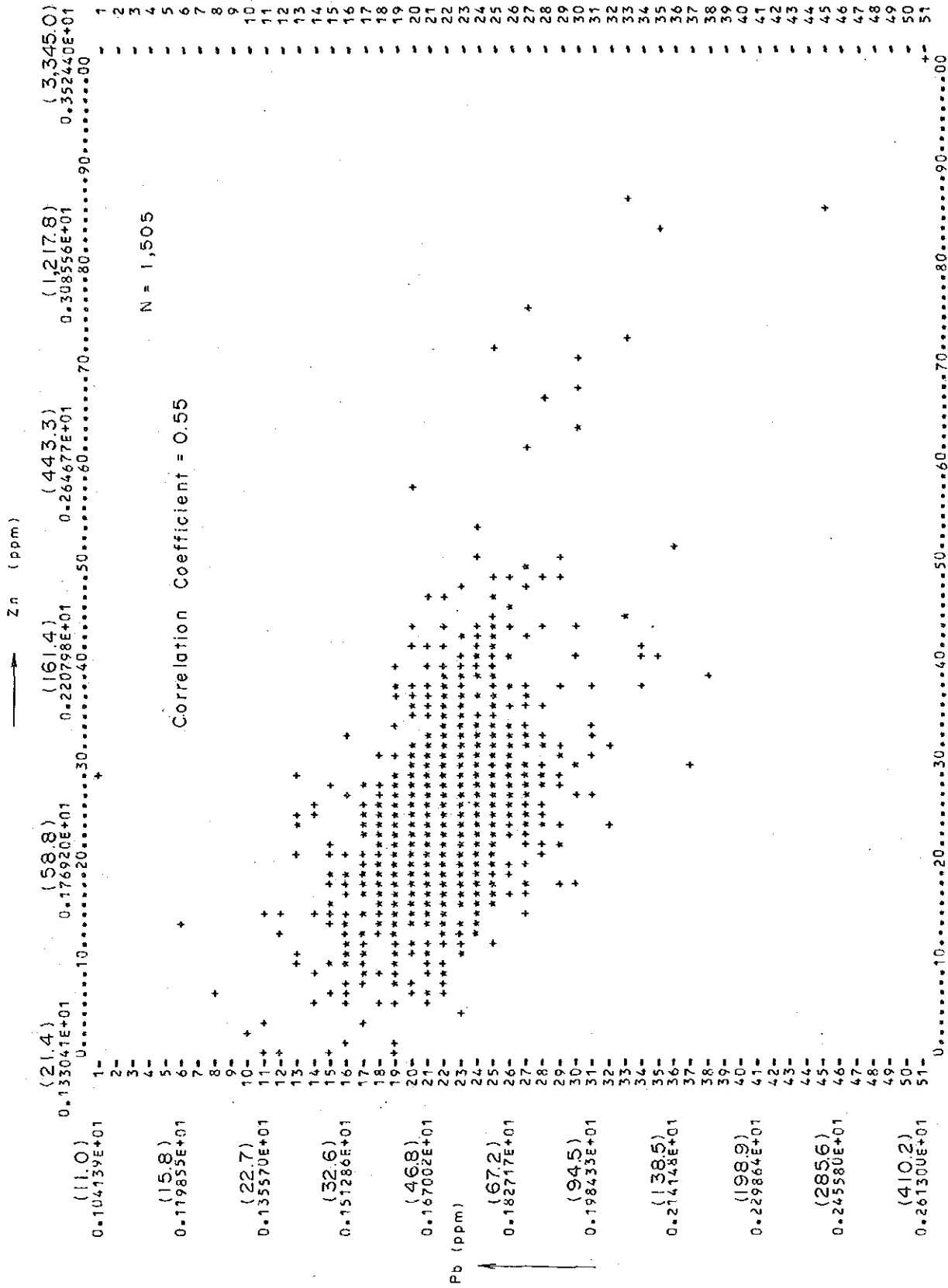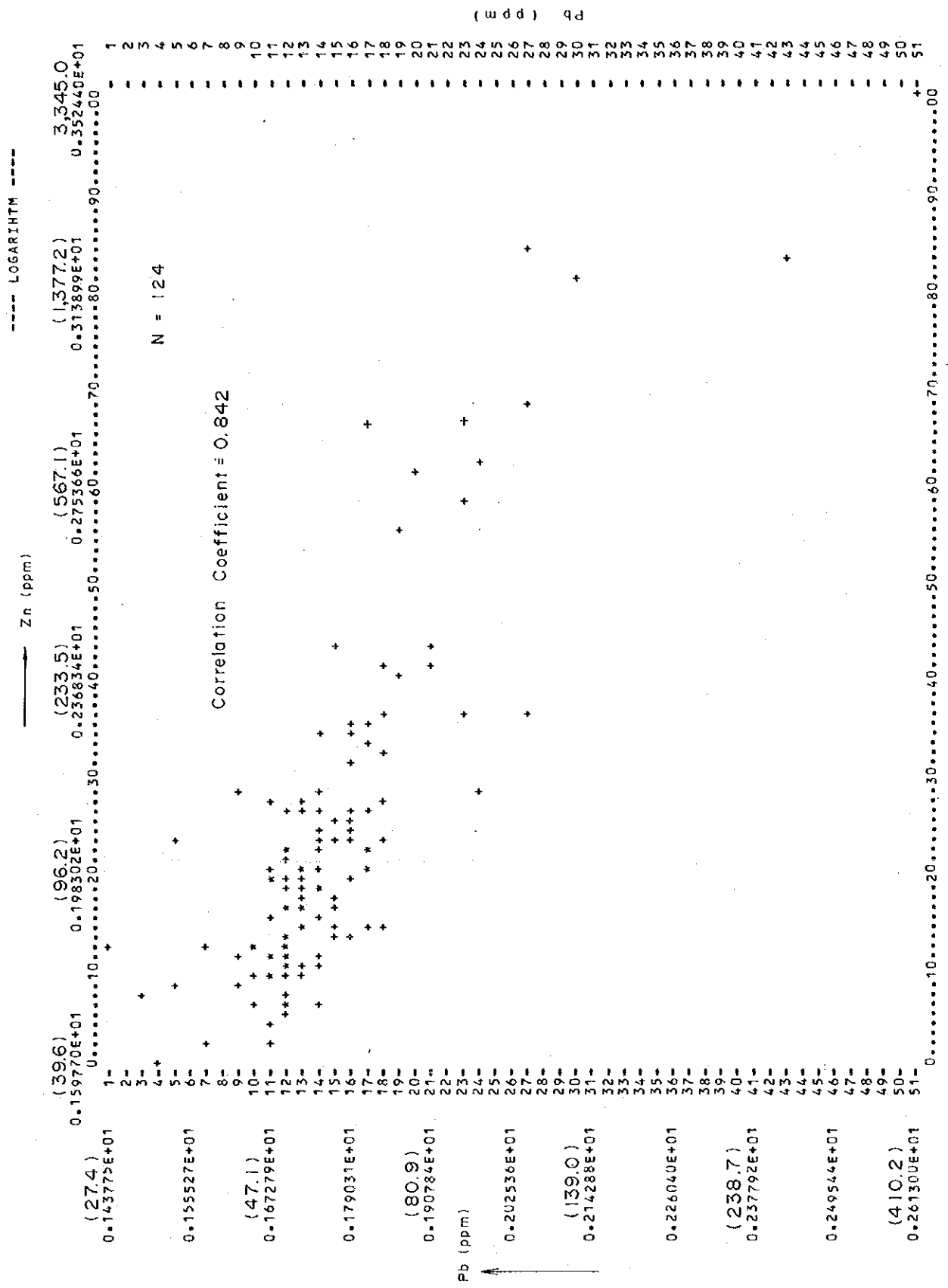Ag: As 66% samples showed values below the detection limit[1], samples were divided into a non-detected group and a detected group. As the Ag contents of the detected group samples are generally low, the distribution of this group is represented as a stepped cumulative frequency curve in relation to the accuracy of the analysis.

In frequency distribution is clearly different from the low content part with 0.54 ppm as a boundary. Therefore, 0.54 ppm was determined as a threshold value for dividing background values and anomalous values.

Cu: In the mode of distribution of the whole rock, the cumulative frequency curve shows negative skewness on the high content side. However, the frequency distribution is clearly different between the low content side and the high content side with 130 ppm as a boundary, so this value was determined as a threshold value. Only five samples showed values above the threshold value, showing poor copper-mineralization in the survey area.

Pb: It shows a log normal distribution with an extremely high degree of concentration. As a distribution of small peaks, which is regarded to be reflecting anomalous populations, begins at 114 ppm towards the high content side, this value was adopted as a threshold value.

Zn: It shows a distribution with a high degree of concentration next to Pb. The clearest positive skewness is observed on the high content side among the four indicators. The frequency curve shows clear difference in the distribution mode of populations between the high content side and the low content side with 365 ppm as a boundary. Therefore, 365 ppm was adopted as a threshold value.

4-1-5 Correlation Coefficient between Indicators

The correlation coefficient between indicators on logarithmic base is shown for the whole rock and each geological unit. In the geological units except the Cretaceous system, correlation coefficients between respective indicators are small, suggesting that the origins of individual indicators are different from each other. However, among the samples originating from the Cretaceous system, the combinations of Pb-Zn, Ag-Zn and Ag-Pb are noticed high correlation coefficient, which is regarded to show that these indicators are those of the same origin, in other words, they are those from the Kuroko type deposit existing in this geological unit.

Using the list of correlation coefficients, tests of 1% and 5% significance levels were carried out (Table 4-2).

---

1) To carry out principal component analysis, values below the detection were handled as 0.01 ppm in statistical treatment.

Table 4 – 2 Matrix of Correlation Coefficient[1]

(Whole Rocks)

	Ag	Cu	Pb	Zn
Ag	1.0 0			
Cu	※※ − 0.1 9	1.0 0		
Pb	※ 0.0 6	※※ 0.2 7	1.0 0	
Zn	※※ 0.2 1	※※ 0.1 8	※※ 0.5 5	1.0 0

※5％Coeff … 0.0 5   ※※1％Coeff … 0.0 7

(Cretaceous System)

1

	Ag	Cu	Pb	Zn
Ag	1.0 0			
Cu	− 0.0 9	1.0 0		
Pb	※※ 0.5 5	0.0 7	1.0 0	
Zn	※※ 0.7 1	0.0 5	※※ 0.8 4	1.0 0

※5％Coeff … 0.1 8   ※※1％Coeff … 0.2 3

(1−Stage Andesites : Tad_1)

2

	Ag	Cu	Pb	Zn
Ag	1.0 0			
Cu	※※ − 0.2 2	1.0 0		
Pb	− 0.0 3	0.1 0	1.0 0	
Zn	※※ 0.3 9	0.0 4	※※ 0.4 8	1.0 0

※5％Coeff … 0.1 6   ※※1％Coeff … 0.2 1

Table 4－2 Matrix of Correlation Coefficent(2)

(Sandstone : Tss₁)

	Ag	Cu	Pb	Zn
Ag	1.0 0			
Cu	※ －0.2 0	1.0 0		
Pb	0.1 6	※ 0.1 9	1.0 0	
Zn	※※ 0.2 6	0.1 5	※※ 0.5 4	1.0 0

※5％Coeff … 0.2　　　　　※※1％Coeff … 0.3

(Ⅱ－Stage Andesites : Tad₂)

	Ag	Cu	Pb	Zn
Ag	1.0 0			
Cu	※※ －0.1 9	1.0 0		
Pb	0.0 2	※※ 0.2 9	1.0 0	
Zn	※ 0.1 5	※※ 0.3 0	※※ 0.5 2	1.0 0

※5％Coeff … 0.1 2　　　　　※※1％Coeff … 0.1 6

(Ⅲ－, Ⅳ－Stage Andesites : Tad₃, Tad₄)

	Ag	Cu	Pb	Zn
Ag	1.0 0			
Cu	※※ 0.1 5	1.0 0		
Pb	－0.0 4	※※ 0.2 7	1.0 0	
Zn	0.0 7	※ 0.1 1	※ 0.4 9	1.0 0

※5％Coeff … 0.0 9　　　　　※※1％Coeff … 0.1 2

Table 4-2 Matrix of Correlation Coefficient (3)

(I-Stage Dacite : Tdc₁)

6

	Ag	Cu	Pb	Zn
Ag	1.0 0			
Cu	0.1 5	1.0 0		
Pb	0.0 9	0.2 0	1.0 0	
Zn	0.0 0	※ 0.2 3	※※ 0.5 5	1.0 0

※5%Coeff ⋯0.2 1   ※※1%Coeff ⋯0.2 8

(Intrusives : Gd, Adm, Gph)

7

	Ag	Cu	Pb	Zn
Ag	1.0 0			
Cu	※ −0.2 0	1.0 0		
Pb	0.0 4	※※ 0.2 8	1.0 0	
Zn	※※ 0.2 4	※※ 0.3 8	※※ 0.3 5	1.0 0

※5%Coeff ⋯0.1 5   ※※1%Coeff ⋯0.2 0

(Others : Tbs₁, etc.)

8

	Ag	Cu	Pb	Zn
Ag	1.0 0			
Cu	−0.1 0	1.0 0		
Pb	0.0 5	※ 0.4 0	1.0 0	
Zn	0.0 4	0.1 4	※※ 0.4 0	1.0 0

※5%Coeff ⋯0.1 5   ※※1%Coeff ⋯0.2 0

4-1-6 Principal Component Analysis

By determining the correlation coefficients between indicators, which cannot be extracted by single variable analyses, from multidimensional distribution characteristics, they were applied to the determination of character and the evaluation of geochemical anomalies (Table 4-3).

Table 4-3 Results of Principal Component Analysis

P·C	Eigen-value	C·R	Eigenvector Ag	Eigenvector Cu	Eigenvector Pb	Eigenvector Zn	Factor Loading Ag	Factor Loading Cu	Factor Loading Pb	Factor Loading Zn	Max. Score	Min. Score
z_1	1.71	0.43	0.14	0.37	0.65	0.64	0.19	0.49	0.85	0.84	12.53	-4.45
z_2	1.20	0.30	0.78	-0.60	-0.03	0.20	0.85	-0.66	-0.03	0.22	4.32	-2.38
z_3	0.66	0.17	0.59	0.71	-0.33	-0.21	0.48	0.58	-0.27	-0.17	2.92	-5.30

P·C : Principal Component
C·R : Contribution Ratio

As shown in this table, the contribution ratio fo the first principal component to all the principal components is about 43%, occupying nearly a half of all. The total to the ratio of the third principal component amounts to 90% approximately, so that a greater part of the fluctuation of all the components can be explained with them. However, compared with the contribution ratio of the second principal component, 30%, that of the third principal component markedly drops to 17%.

Factor loading is composed of correlation coefficients between principal components and variables (indicator contents). For the first principal component, Pb-Zn shows a high value 0.85-0.84, but Cu shows 0.49 reduced to nearly a half. Therefore, the first principal component is characterized by high correlation with Pb and Zn and medium degree of correlation with Cu.

The second principal component is characterized by the high correlation (0.85) with Ag and the negative correlation (-0.66) with Cu. The third principal component has medium degrees of correlation with Ag and Cu and must show high scores in samples with indicator contents not correlated with Pb and Zn. However, there are few geochemical anomalies with a structure characterized by the third principal component.

4-1-7 Evaluation of Geochemical Anomaly using Stream Sediments

Anomalous zones in the survey area can be classified into single element showing type ones and multi-element showing type ones according to the combinations of indicators which show anomaly.

The explanation and evaluation of anomalous zones are carried out besed on referring the structures of the first to third factor loading, factor score and contrast. The results are described as follows.

(1) Single Element Showing Type-Ag

This type seems to be divided again into three types, a type which shows the mineralization of Ag only (the mineralization of Cu, Pb and Zn is not accompanied or is weak) and the score of the first principal component near zero, and types which accompany the mineralization of Cu or Zn although to a low degree.

The characteristics of each anomalous zone are as shown in Table 4-4.

Table 4－4 Evaluation of Anomalous Zones (Ag)

Anomalous Zones	Sample No.	R·C	Contents of Indicators (ppm)				P.C. A'S Score			Inferred Type of Mineralization
			Ag	Cu	Pb	Zn	Z1	Z2	Z3	
Tierra Coloradas-N	172	6	0.9 (11)	46.7 (7.3)	71.3 (1.4)	118.1 (1.8)	2.211	1.381	1.538	Ag-(Cu) mineralization
El Crucero	214	8	0.6 (10)	13.7 (1.1)	44.8 (0.9)	189.1 (2.7)	1.229	2.032	1.062	Ag-(Zn) mineralization
Tierra Coloradas	390	6	0.6 (7.5)	40.6 (6.3)	77.5 (1.5)	93.5 (1.4)	2.016	1.123	1.285	Ag-(Cu) mineralization
San Carlos	427	5	1.1 (37)	46.9 (5.6)	67.9 (1.3)	93.8 (1.3)	1.776	1.389	1.792	Ag-(Cu) mineralization
	706	5	1.2 (40)	50.9 (6.1)	75.8 (1.5)	97.0 (1.3)	2.148	1.398	1.712	
Para Nada	457	8	2.5 (42)	12.5 (1.0)	68.1 (1.3)	98.5 (1.4)	1.522	2.506	1.318	Ag mineralization
La Yerba Buena-W	509	2	0.7 (50)	40.8 (0.9)	81.5 (1.5)	250.5 (3.5)	3.565	1.634	0.835	Ag-(Zn) mineralization
Puerto del Colomo	695	8	0.6 (10)	4.7 (0.4)	49.0 (1.0)	46.7 (0.7)	0.853	1.936	0.947	Ag mineralization
La America-S	820	1	0.7 (23)	15.4 (0.6)	70.3 (1.2)	244.7 (2.1)	2.838	2.124	0.470	Ag-(Zn) mineralization
Chambueres	877	5	1.1 (37)	6.2 (0.7)	50.9 (1.0)	96.2 (1.3)	0.419	2.437	0.975	Ag mineralization
San Agustin	1364	5	1.9 (63)	2.6 (0.3)	88.7 (1.7)	52.8 (0.7)	0.819	2.839	0.210	Ag mineralization
San Agustin-N	1389	5	1.1 (37)	3.2 (0.4)	67.1 (1.3)	49.8 (0.7)	0.009	2.447	0.513	Ag mineralization

(7.3) : Contrast (Ratio of background value of geological unit to threshold)

R·C: Rock code (R·Conumber Shown in Table 4－1)

P.C.A'S: Principal Component Analysis's

These anomalous zones are usually found in Tertiary volcanic rocks (III-IV stage andesites, I-stage dacites, etc.), and in this case, they are characterized by the mineralization of Ag only or that of Ag-(Cu). On the other hand, those found in or near the Cretaceos system are characterized by the mineralization of Ag-(Zn).

(2) Single Element Showing Type-Cu

This type anomalous zone is found only around Cerro San Pedro and shows the mineralization of Cu only. The geology dominating the anomalous zone is composed of I-stage andesites (Tad$_1$) and granodiorite (Gd), but it is difficult to suppose the origin of the mineralization.

The small exposed parts of granophyre are found near the anomalous zone and concealment near here is expected, but no occurrence showing direct relationship with this anomalous zone was observed. The characteristics of each anomalous zone are as shown in Table 4-5. They are characterized by the low scores (low Ag, high Cu) of the second factor.

Table 4-5 Evaluation of Anomalous Zones (Cu)

Anomalous Zones	Sample No.	R C	Contents of Indicators(ppm)				P.C. A'S Score			Type of Inferred Mineralization
			Ag	Cu	Pb	Zn	z_1	z_2	z_3	
San Pedro	739	2	0.01 (0.7)	145.5 (3.0)	49.5 (0.9)	53.3 (0.7)	0.028	-1.897	1.005	Cu-mineralization
	744	7	0.01 (0.6)	138.0 (14)	56.6 (1.1)	76.8 (1.2)	0.884	-1.723	0.862	
	787	2	0.01 (0.7)	135.7 (2.9)	52.6 (1.0)	58.0 (0.8)	0.287	-1.831	1.079	
	788	2	0.01 (0.7)	231.5 (4.9)	41.2 (0.8)	28.9 (0.4)	-1.182	-2.381	2.039	

(3) Single Element Showing Type-Pb

With this type anomalous zones, San Pedro-NW area and Arroyo El Narranjo area form geochemically similar anomalous zones regardless of geological difference. The mineralization inferred by them will be of a type accompanying that of a certain degree of Cu nd Zn. In the case of the latter, the anomalous zone is shown by plural geochemically similar samples but is different from the multi-element showing type found around a Kuroko type deposit in the structure of principal component scores.

The anomalous zone in Arroyo Las Palmas area and that in Cruz Gorda-W area are similar to each other in their indicator contents and factor scores, and may accompany weak Ag mineralization. Table 4-6 shows the characteristics of anomalous zones.

Table 4-6 Evaluation of Anomalous Zones (Pb)

Anomalous Zones	Sample No.	RC	Contents of Indicators(ppm)				P.C. A'S Score			Type of Inferred Mineralization
			Ag	Cu	Pb	Zn	Z_1	Z_2	Z_3	
San Pedro-NW	726	1	0.01 (0.3)	48.3 (1.7)	114.9 (2.0)	202.8 (1.7)	3.808	-0.842	-1.150	Pb-(Cu)-(Zn) minerali-zation
	727	2	0.01 (0.7)	51.5 (1.1)	117.9 (2.2)	199.5 (2.7)	3.873	-0.883	-1.139	
Arroyo las Palmas	990	3	0.1 (5.6)	14.9 (0.7)	161.0 (3.0)	152.4 (2.1)	4.155	0.810	-1.235	Pb-(Pb?)-(Zn) mineraliza-tion
Arroyo el Naranjo	1437	4	0.01 (0.5)	74.4 (6.2)	139.4 (2.7)	289.6 (3.9)	4.960	-0.919	-1.317	
	1438	4	0.10 (5.0)	29.6 (2.5)	123.0 (2.4)	140.0 (1.9)	3.536	0.458	-0.430	
	1439	4	0.01 (0.5)	45.7 (3.8)	120.6 (2.3)	170.8 (2.3)	3.675	-0.895	-1.169	Pb-(Cu)-(Zn) mineraliza-tion
	1478	4	0.01 (0.5)	27.5 (2.3)	136.9 (2.6)	168.7 (2.3)	3.835	-0.660	-1.633	
	1483	4	0.01 (0.5)	24.2 (2.0)	127.6 (2.5)	167.8 (2.2)	3.601	-0.592	-1.612	
Cruz Gorda-W	1495	5	0.10 (3.3)	19.9 (2.4)	149.8 (2.9)	97.4 (1.3)	3.418	0.475	0.764	Pb-(Ag?)-(Cu)-(Zn) mineralization

(4) Single Element Showing Type-Zn

These anomalous zones found in and around the La America-Descubridora area are classified into the single element showing type group, but all show high Ag contrast which is judged to be the sign accompanying Ag mineralization (Table 4-7). Therefore, they are similar to the multi-element showing type (Ag-Zn anomaly) found around a Kuroko type deposit.

Table 4-7 Evaluation of Anomalous Zones (Zn)

Anomalous Zones	Sample No.	RC	Contents of Indicators(ppm)				P.C. A'S Score			Type of Inferred Mineralization
			Ag	Cu	Pb	Zn	Z_1	Z_2	Z_3	
Descubridora	821	1	0.2 (6.7)	37.0 (1.3)	75.9 (1.3)	467.3 (4.0)	4.109	1.299	0.083	Zn-(Ag) mineralization
Arroyo las Palmas-N	961	3	0.2 (11)	25.3 (1.3)	91.7 (1.7)	525.5 (7.3)	4.657	1.521	-0.449	Zn-(Ag) mineralization

(5) Multi-Element Showing Type (Composite Type) - Ag, Cu, Pb, Zn

This type anomalous zones appear characteristically in most cases in or around areas containing Kuroko type deposits. The showing indicator is basically the combination of Ag-Zn, and Cu and Pb add to it. This type is characterized by the high scores of the first principal component and the medium degree scores of the second principal component. There is no direct relationship between these geochemically anomalous zones and Kuroko type deposits, and these zones are highly possible to have caught the result of subsequent mineralization which succeeded the principal mineralization that formed the Kuroko type deposits. The mineralized signs of Ag and Zn were noticed in the hanging wall dacite

Table 4-8 Evaluation of Anomalous Zones (Composite Type)

Anomalous Zones	Sample No.	R.C	Contents of Indicators(ppm)				P.C. A's Score			Type of Inferred Mineralization
			Ag	Cu	Pb	Zn	Z1	Z2	Z3	
Espinos ? Pena	349	7	0.7 (41)	46.6 (4.8)	44.7 (0.9)	391.0 (6.2)	2.651	1.827	1.519	Ag-Zn-(Cu) mineralization
El Rubi-E	490	1	8.1 (270)	477.7 (17)	410.2 (7.0)	3,345 (29)	12.526	2.697	-0.077	Ag-Cu-Pb-Zn mineralization
La America	765	1	0.2 (6.7)	0.2 (0.01)	276.5 (4.7)	1,627 (14)	7.673	4.320	-5.299	Pb-Zn-(Ag) mineralization
Descubridora-N	812	1	2.9 (97)	62.8 (2.2)	117.3 (2.0)	1,666 (14)	7.493	2.979	0.313	Ag-Pb-Zn-(Cu) mineralization
Aranjuez-NE	797	1	5.3 (177)	40.0 (1.4)	131.8 (2.3)	1,441 (12)	7.514	3.449	0.200	Ag-Pb-Zn mineralization
Aranjuez-E	808	1	2.1 (70)	29.4 (1.1)	112.7 (1.9)	833.4 (7.2)	6.135	2.882	0.104	
	813	1	1.0 (33)	19.9 (0.7)	79.5 (1.4)	610.6 (5.3)	4.576	2.579	0.184	Ag-Zn-(Pb) mineralization
	814	1	2.5 (83)	72.7 (2.6)	96.4 (1.6)	633.9 (5.5)	5.633	2.419	1.042	
La Queseria-S	823	1	0.8 (27)	39.8 (1.4)	76.5 (1.3)	990.1 (8.5)	5.355	2.333	0.335	
	824	1	0.9 (30)	34.3 (1.2)	95.0 (1.6)	526.7 (4.5)	4.997	2.168	0.290	Ag-Zn mineralization
	1139	1	0.6 (20)	23.5 (0.8)	64.7 (1.1)	773.4 (6.7)	4.369	2.350	0.245	
Descubridora-S	957	1	2.3 (77)	25.6 (0.9)	91.3 (1.6)	753.6 (6.5)	5.402	2.977	0.388	

(Tdc_2) of La America-Descubridora area. Table 4-8 shows the geochemical characteristics of this type anomalous zones.

The anomalous zone in the Espinos Pina area is different from other anomalous zones in the factor scores and cannot be regarded as Kuroko type mineralization.

As discussed above, the geochemical anomalies found in an area containing Kuroko type deposits are multi-element showing type based on the combination of indicators, principally Ag-Zn, and can be clearly distinguished from the single element showing type dominant in other areas. These anomalies may not be directly originating from the Kuroko type mineralization but are highly possible to be showing, so to speak, subsequent Kuroko mineralization which succeeds the principal mineralization of the Kuroko type, and are important in the point it shows the existence of Kuroko mineralization although indirectly.

4-2　Geochemical Exploration by Whole Rock Analysis

Various attempts (for example, Dudas, 1983; Hashimoto, 1983) have been made to distinguish volcanic rock related with Kuroko type deposits in their origin from those not related from a lithogeochemical standpoint, but perfect solution has not been given to this problem in results regardless of the principal elements or the minor elements of rocks. In this survey, this problem was studied taking the foot wall dacite (Kdc_1), the pyroclastics of ore horizon (Koh), the hanging wall dacite (Kdc_2) and other dacites (Tdc_1, Tdc_3) with alteration signs, which are distributed around known Kuroko type deposits, and the dacite intercalated in the IV-stage andesites (Tad_4).

Using the 13 main components in 102 rock samples collected, (1) presumption of volcanic rock series, (2) Study on alkali alteration index, (3) principal component analyses and (4) cluster analyses were carried out. About the latter two, the manner of difference of geology in sampling sites on geochemical characteristics was investigated.

4-2-1　Presumption of Volcanic Rock Series

About the samples in which formation of altered minerals was not noticed or noticed very little, the volcanic series to which these samples belong were supposed using Figs. 4-8 and 4-9. The triangular diagram shown in Fig. 4-8 is useful for the classification of rock series and also represents the change of crystallization differentiation. As it is usually thought that MgO concentrate into rocks which crystallize in earlier stages, the composition of magma is changed gradually from the corner of MgO to the lower left corner (Na_2O + K_2O) as crystallization differentiation proceeds. The four samples shown in Fig. 4-8 are all regarded to be those formed in the later stages of differentiation. Especially, the hanging wall dacite of El Rubi deposit is thought to be the latest stage of differentiation. As shown in Fig. 4-9, the hanging wall dacite (Kdc_2) of the upper Cretaceous system and Tertiary dacite (Tdc_1) are all plotted in the calc-alkaline rock series region on the $FeO^*-(FeO^*/MgO)$ relation diagram except one example plotted in the theleiitic rock series region. This fact supports the idea (for example, Lambert & Sato, 1974) to interpret that Kuroko type deposits are related with calc-alkaline rock series. It also agrees with the fact that the dominant rock series of two great volcanic zones (Sierra Madre Occidental and Eje Neovolcanico) in the United Mexican States seem to be calc-alkali rock series (Nieto et al., 1981).
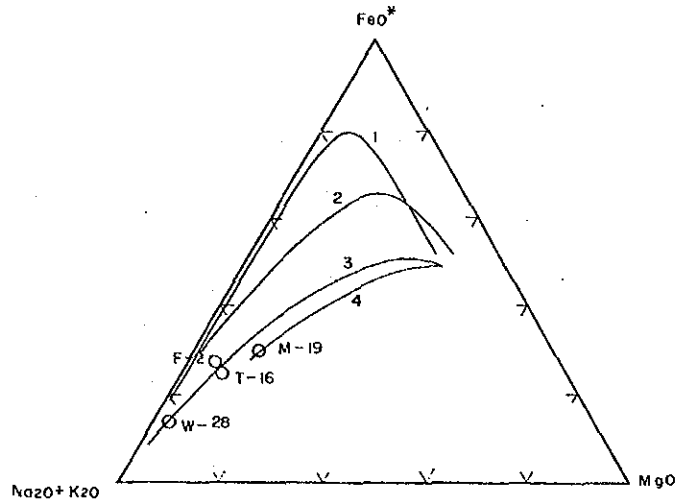
Fig. 4-8   MgO - FeO* - (Na₂O + K₂O) Diagram

1. Skaergaad magma
2. Averaged tholeiitic volcanic rocks of Izu islands , Izu peninsula and Hakone region
3. Averaged Calc - alkaline volcanic rocks of Izu islands , Izu peninsula and Hakone region.
4. Calc - alkaline volcanic rocks of Mt. Akagi
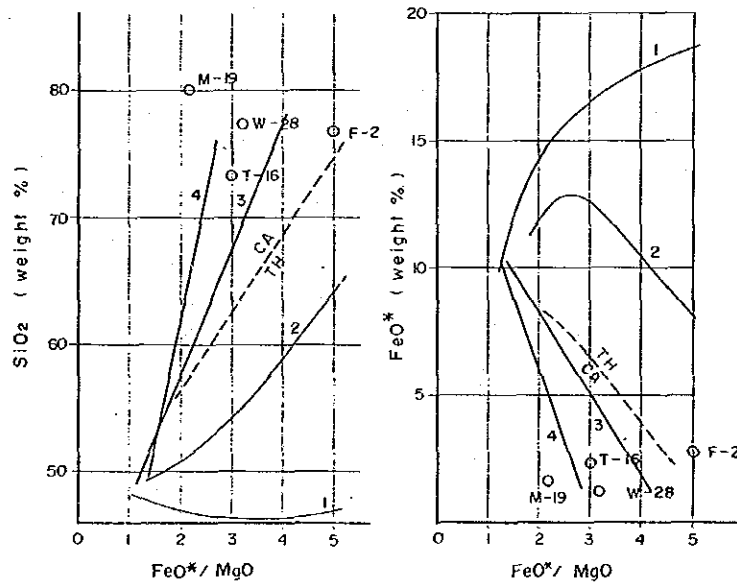
FeO* : Total Fe as FeO

Fig. 4-9   Classification of Calc-alkaline and Tholeiitic
Rock Series by FeO*/MgO

CA   : Calc - alkaline rock series
TH   : Tholeiitic rock series

4-2-2 Alkali Alteration Index*

In the case of Japanese Cenozoic Kuroko deposits, altered zones are generally evaluated using the foot wall dacite, which is regarded to have received the influence of hydrothermal alteration at the time of ore formation most seriously (Hashiguchi et al., 1981). As the area of foot wall dacite (Kdc_1) distribution is small in this survey area, alteration was evaluated using the hanging wall dacite (Kdc_2) and the pyroclastics of ore horizon, which are both distributed in comparatively wide areas. Also a certain amount of investigation was made about Tertiary dacites (Tdc_1, Tdc_3, etc.) whose alteration is noticed in comparatively compact areas.

The alkali alteration index is an index devised for the quantitative re-presentation of the degree of alteration paying attention to the high responsiveness of alkali and alkaline earth elements to hydrothermal alteration and greatly contributed to the discovery of Ezuri deposit, a Japanese Cenozoic Kuroko deposit, by Ishikawa et al. (1980).

For the movement of elements by Kuroko type alteration, commonness is noticed apart from the formation time and the distribution of deposits (Table 4-9). Especially, the addition and leach of alkali and alkaline earth elements are character-istics.

As the La America and Descubridora depositis are also regarded to be Kuroko type deposits, the mode of alteration accompanied by these deposits was investigated from the viewpoint of alkaline alteration index.

(La America-Descubridora Area)

Two inensely altered zones (alkali alteration index above 90%) stretching in the NE-SW direction are noticed in the distribution areas of hanging wall dacite (Kdc_2) and the pyroclastics (Koh) of ore horizon, and these two zones are bounded by a weak alteration zone of the alteration index of 50 - 60%. La America deposit is included in the intense alteration zone, but Descubridora deposit corresponds rather to the weak alteration zone. The development of the two intensely altered zones towards southwest has not been interrupted in both cases and the development can be expected (Fig. 4-10). In relation to the low resistivity zones by the CSAMT method, which were found around this area, the intensely altered zones are open to the low resistivity zone situated in the southwestern part of the Descubridora deposit.

(El Rubi Area)

Although the distribution of foot wall dacite (Kdc_1) and hanging wall dacite (Kdc_2) have been limited, intense alteration zone and fairly intense alteration zone (above 80%) are observed in the central part of the hanging wall dacite as shown in Fig. 4-11. Also in the exposed part of the foot wall dacite (Kdc_1), a fairly intense alteration part is noticed locally, but in the eastern extensions of both the hanging wall and foot wall dacites, the degree of alteration becomes weaker (Fig. 4-11).

---

* Alkali Alteration Index = $(MgO + K_2O)/(MgO + K_2O + Na_2O + CaO)$ x 100
( ) weight %

Table 4-9 Major Element Dispersions in relation to Kuroko Type Deposits

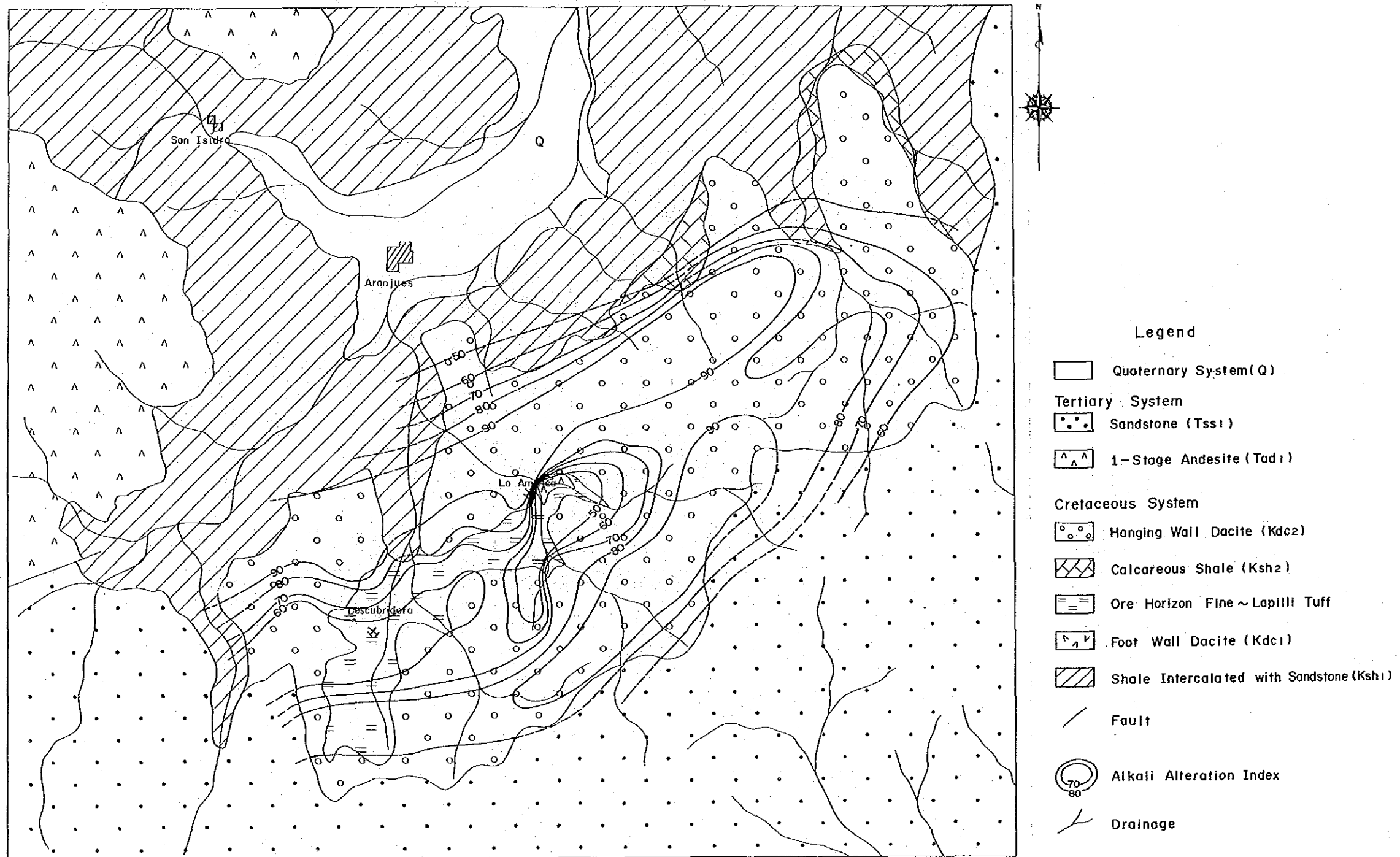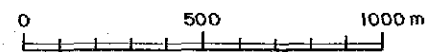|	Alteration mineralogy	Elements enriched	Elements depleted	Elements unchanged	Age
Kuroko, Japan Lambert & Sato (1974)	Mon,Ser,Chl, Kaol.	K,Mg,Fe,Si	Na,Ca		Cenozoic
Kuroko, Japan Tatsumi & Clark (1972)	Ser,Qtz, Cal	Mg,K	Na,Ca,Fe	Al	Cenozoic
Hitachi, Japan Kuroda (1961)	Cord, Anthoph.	Mg,Fe,Ba	Na,Ca,Sr		Cenozoic
Buchans, Canada Thurlow et al. (1975)	Chl,Ser, Qtz	Mg,Fe,Si	Na,Ca,K		Paleozoic
Heath Steele, Canada Wahl et al. (1975)	Chl,Ser	Mg	Na,Ca		Paleozoic
Brunswick No.12 Canada Goodfellow (1975)	Chl,Ser, Qtz	Mg,Fe,(Mn), (K)	Na,Ca (Mn),(K)	Al	Paleozoic
Killingdal, Norway Rui (1973)	Chl,Bio, Qtz	Mg,K,Mn	Na,Ca,Si	Al,Ti, Fe(total)	Paleozoic
Skorovass, Norway Gjelsvik (1968)	Chl,Ser	Mg	Na,Ca		Paleozoic
Boliden, Sweden Nilsson (1968)	Chl, Ser, Qtz,Andal	Mg,K,Al	Na,Ca		Proterozoic
Mattabi, Canada Franklin et al. (1975)	Qtz,Carb, Ser,Chld, Chl,Andal, Gar,Kyan, Bio	Fe,Mg	Na,Ca		Archean
Millenbach, Canada Simmons et al. (1973)	Chl,Ser, Anthoph, Cord.	Mg,Fe	Na,Ca,Si		Archean
Mines de Poirier Canada Descarreaux (1973)	Chl,Ser,	Mg,K	Na,Ca	Si	Archean
Lac Dufault, Canada Sakrison (1966)	Chl,Ser	Mg,Fe,Mn	Na,Ca	Al,Ti K,Si	Archean
East Waite, Mobrun, Joutel, Poirier, Agnico-Eagle, Mattabi, Sturgeon Lake, South Bay McConnell (1976)	Qtz,Ser,Chl, Carb, Sauss, Epidote	Mg,Fe	Na,Ca	Si,Al	Archean

(After Govett & Nichol, 1979)

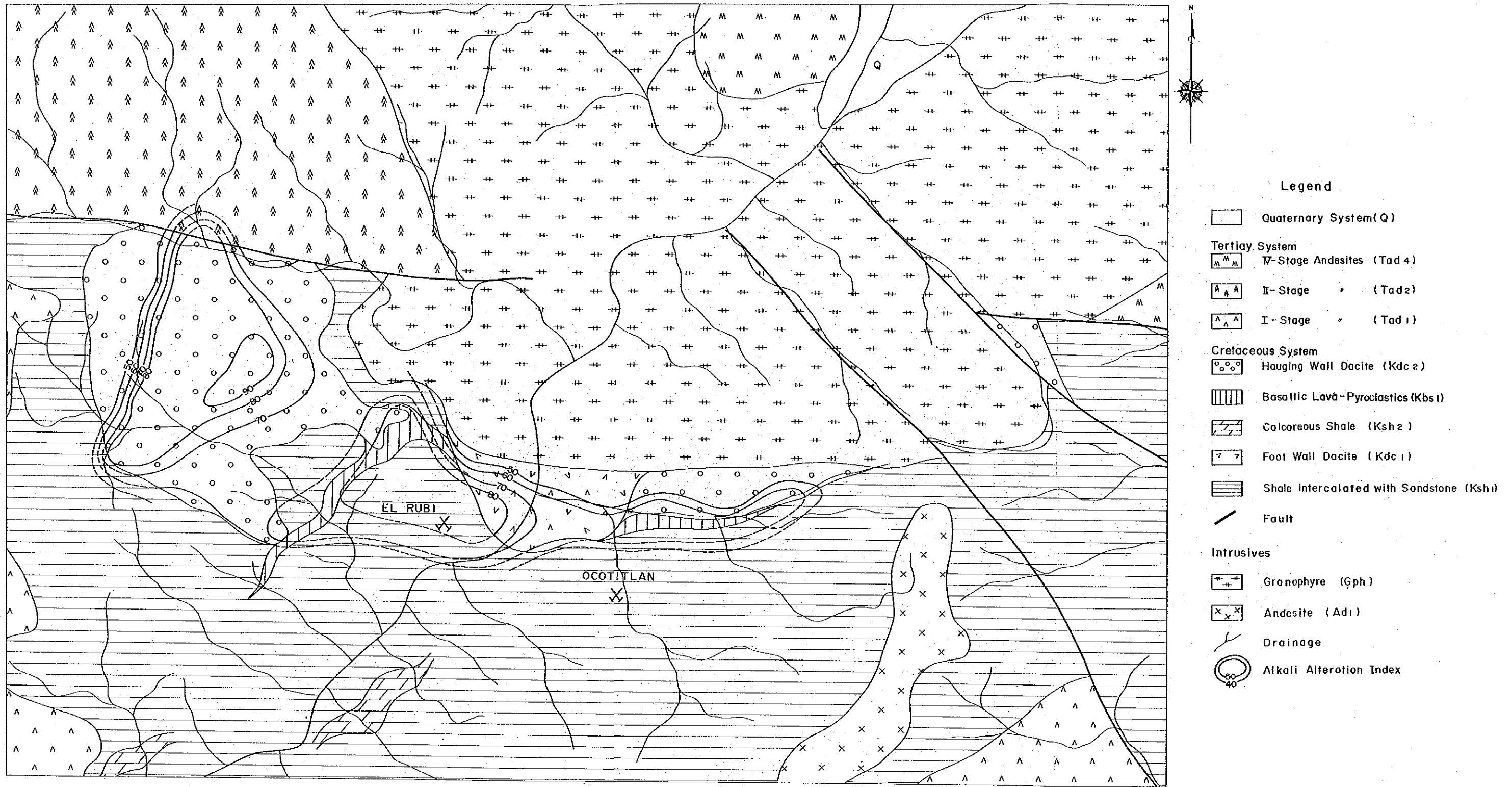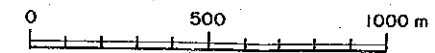Fig. 4-10 Alkali Alteration Index in La America - Descubridora Area

Legend

	Quaternary System (Q)
	Tertiary System
	Sandstone (Tss1)
	1-Stage Andesite (Tad1)
	Cretaceous System
	Hanging Wall Dacite (Kdc2)
	Calcareous Shale (Ksh2)
	Ore Horizon Fine ~ Lapilli Tuff
	Foot Wall Dacite (Kdc1)
	Shale Intercalated with Sandstone (Ksh1)
	Fault
	Alkali Alteration Index
	Drainage

0   500   1000 m

Fig. 4-11 Alkali Alteration Index in El Rubi Area

Legend

Quaternary System (Q)

Tertiay System
- Ⅳ-Stage Andesites (Tad 4)
- Ⅱ-Stage ⁗ (Tad 2)
- Ⅰ-Stage ⁗ (Tad 1)

Cretaceous System
- Hauging Wall Dacite (Kdc 2)
- Basaltic Lava-Pyroclastics (Kbs 1)
- Calcareous Shale (Ksh 2)
- Foot Wall Dacite (Kdc 1)
- Shale intercalated with Sandstone (Ksh 1)
- Fault

Intrusives
- Granophyre (Gph)
- Andesite (Ad 1)
- Drainage
- Alkali Alteration Index

EL RUBI

OCOTITLAN

0   500   1000 m

When judged from the alkali alteration index, the intense and fairly intense alteration zones in the hanging wall dacite (Kdc$_2$) can also be regarded as a separate alteration zone from the alteration zone which formed the known El Rubi deposit, and the existing El Rubi deposit is included in the fairly intense alteration zone in the southeastern part of this intense alteration zone.

(Rincon Area)

This is an alteration zone in I-stage dacite (Tdc$_1$) of the Tertiary in this area. An intense alteration zone of a scale of 400 m x 500 m is noticed.

However, the zone seems to change into a weak alteration zone immediately around it. Among other samples in the same rock formation, there are no samples of intense alteration to be noted particularly, therefore, the zone will be an alteration zone limited in this area. The behaviors of alkali and alkaline earth elements are similar to those in the case of the Kuroko type alteration, but as a result of the cluster analysis described later, few positive reasons were noticed to include this alteration in the Kuroko type alteration.

4-2-3 Principal Component Analysis

For the main 13 components in 102 rock samples collected in the survey area, principal component analyses were carried out to clarify the relationship with the Kuroko type mineralization. Correlation coefficients for the 13 components are shown in Table 4-10.

In this table, correlation is noticed in the following combinations.

$$P_2O_5 \ - \ Al_2O_3 \quad (0.79)$$
$$MgO \ - \ FeO \quad (0.78)$$
$$CaO \ - \ Na_2O \quad (0.60)$$
$$BaO \ - \ K_2O \quad (0.59)$$
$$MnO \ - \ FeO \quad (0.52)$$
$$Na_2O \ - \ Al_2O_3 \quad (0.47)$$
$$CaO \ - \ MnO \quad (0.46)$$
$$MgO \ - \ MnO \quad (0.45)$$

Also, negative correlation between SiO$_2$ and the following elements is noticed.

$$SiO_2 \ - \ Al_2O_3 \quad (-0.83)$$
$$SiO_2 \ - \ Na_2O \quad (-0.46)$$
$$SiO_2 \ - \ TiO_2 \quad (-0.46)$$
$$SiO_2 \ - \ MnO \quad (-0.40)$$

Correlation is noticed between CaO and Na$_2$O which have strong leaching tendency when subjected to hydrothermal alteration, and between BaO and K$_2$O with strong increasing tendency.

Table 4-10 Matrix of Correlation Coefficient

	SiO_2	TiO_2	Al_2O_3	Fe_2O_3	FeO	MnO	MgO	CaO	Na_2O	K_2O	P_2O_5	LOI	BaO
SiO_2	1.00												
TiO_2	−0.46	1.00											
Al_2O_3	−0.83	0.31	1.00										
Fe_2O_3	−0.19	0.32	0.14	1.00									
FeO	−0.15	0.09	−0.05	−0.15	1.00								
MnO	−0.40	0.33	0.23	0.17	0.52	1.00							
MgO	−0.18	0.13	0.45	−0.05	0.78	0.45	1.00						
CaO	−0.21	0.12	0.09	−0.12	0.39	0.46	0.38	1.00					
Na_2O	−0.46	0.20	0.47	0.08	0.12	0.30	0.10	0.60	1.00				
K_2O	−0.33	0.07	0.40	0.09	−0.23	0.03	−0.32	−0.35	−0.13	1.00			
P_2O_5	−0.39	0.79	0.18	0.26	0.24	0.32	0.18	0.20	0.13	0.07	1.00		
LOI	−0.37	0.19	0.16	0.13	0.18	0.18	0.34	−0.03	−0.18	−0.07	0.07	1.00	
BaO	−0.22	−0.09	0.19	0.14	−0.02	0.15	−0.12	−0.09	−0.06	0.59	0.12	0.20	1.00

Correlation holds also between MgO and FeO with which geochemically similar behaviors are expected as the components of rocks.

About the components which show negative correlation, the leaching tendency of Na_2O for increase in SiO_2 (silicification), etc., is shown.

After standardizing the value of each component, principal component analyses were carried out. The results are shown in Table 4-11.

According to this table, the maximum eigenvalue is 3.66, which is the square sum of the first factor loading, so a 28% of the whole can be explained with this first factor. When calculated in the same way for the second and the third factors, 19% and 12% are determined and 11%, for the fourth eigenvalue. Therefore, a 71% of the original data used for this analysis can be explained with the first to fourth eigenvalues.

When the factor loading, which is regarded most important in this analysis, is observed, Z_1 is characterized by negative correlation of SiO_2 with other components. It shows that when SiO_2 is increased by silicification, other components have strong tendency to decrease relatively.

Generally, silicification includes two types, one is to add silica and the other is that relative increase in silica occurs as a result of leaching of components other than silica. In the survey area, the former case is supported from the results of principal component analysis and the field occurrence.

Z_2 is characterized by the non-correlation of the petrological basic elements such as FeO, MgO and CaO with K_2O, Al_2O_3 and BaO.

K_2O, which is most highly correlated with Z_2, shows, in the case of Kuroko type alteration, a tendency of remarkable increase with the progress of the alteration, and has character to assume a opposite behavior with Na_2O. Therefore, negative correlation can be expected, but this principal component analysis showed non-correlation merely between Na_2O and K_2O.

About Z_3, the high correlation (0.75) with Na_2O is noticeable. It can be ranked as the principal component for explaining the behaviors of Na_2O which reacts most sensitively for hydrothermal alteration.

About the principal components from Z_4 and lower, positive correlation of medium order of Z_4 with TiO_2 and P_2O_5, about Z_5, negative correlation of medium order with LOI, about Z_6, positive correlation of medium order with Fe_2O_3 are only noticed, and it is difficult to give petrological meaning.

For alteration, the distribution of each sample in the two-dimensional space due to the second and the third factor scores, to which alkali and alkaline earth elements most sensitive to alteration seem to contribute greatly, was investigated (Fig. 4-12).

Especially, attention was paid to the mutual distribution relation resulting from difference in the geological units of sampling sites. The geological units are as follows.

A :   Hanging wall dacite (Kdc$_2$, La America-Descubridora Area)

B :   Hanging wall decite (Kdc$_2$, El Rubi Area)

Table 4 — 11　Analytical Results of Principal Component Analysis

P.C	E.V	C.R	Factor Loading													Max. Score	Min. Score
			SiO_2	TiO_2	Al_2O_3	Fe_2O_3	FeO	MnO	MgO	CaO	Na_2O	K_2O	P_2O_5	LOI	BaO		
Z_1	3.66	0.28	-0.78	0.64	0.59	0.25	0.52	0.72	0.54	0.54	0.54	0.04	0.63	0.37	0.12	5.15	-6.88
Z_2	2.52	0.48	0.42	0.20	0.53	0.35	0.59	0.17	0.59	0.49	0.06	0.79	0.12	0.03	-0.53	4.11	-3.22
Z_3	1.56	0.60	-0.12	0.12	0.31	0.16	0.30	0.09	0.33	0.41	0.75	0.11	0.22	0.59	-0.28	3.99	-2.85
Z_4	1.47	0.71	0.15	0.62	0.20	0.40	0.28	0.18	0.21	0.12	0.05	0.32	0.54	0.12	-0.54	3.01	-3.30
Z_5	0.98	0.78	0.29	0.05	0.34	0.14	0.17	0.35	0.10	0.15	0.01	0.28	0.23	0.56	0.35	2.15	-4.02
Z_6	0.88	0.85	0.08	0.21	0.11	0.71	0.16	0.14	0.02	0.13	0.17	0.25	0.27	0.22	0.18	2.06	-3.86

P・C : Principal components

E・V : Eigenvalue

C・R : Contribution ratio

LOI : Loss on ignition
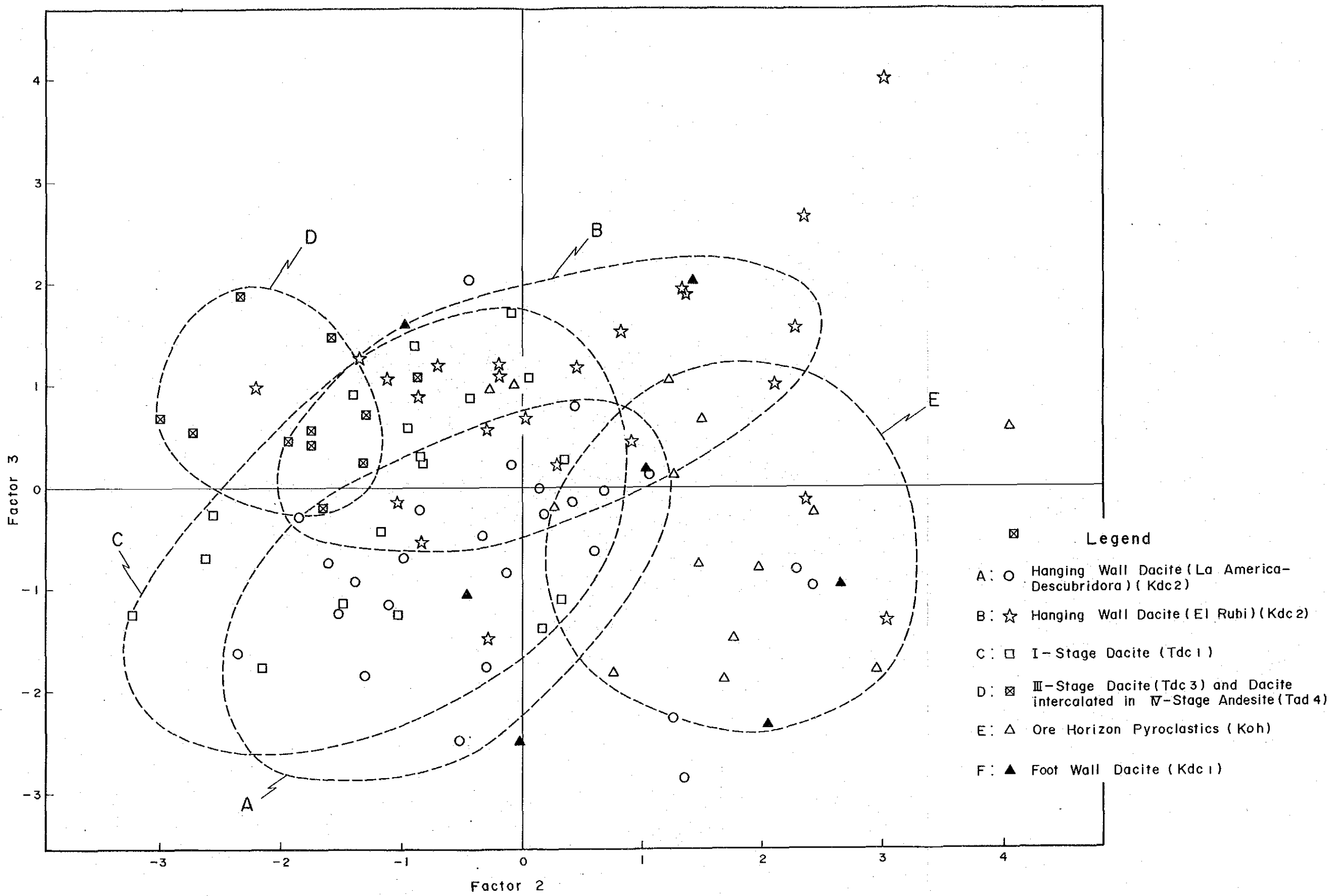
Fig.4-12 Relation Between Factor 2 and Factor 3

C : I-stage dacite (Tdc₁)

D : III-stage dacites (Tdc₃), etc.

E : Ore horizon pyroclastics (Koh)

F : Foot wall dacite (Kdc₁)

According to these unit, the distribution areas of D group and E group are separated not overlapping with each other. With the second principal component, while the former is characterized with a negative value, a greater part of the latter have positive scores, so that the two can be distinguished clearly from each other.

A, B, and C groups are distributed in the zone between D and E groups overlapping with each other, and it is difficult to distinguish them clearly based on the scores of respective factor scores. Especially, A and C groups overlap with each other greatly and they can be said to have similar character in the distribution of two scores.

The foot wall dacite (Kdc₁) is distributed over a wide area in the figure and its characteristics cannot be specified.

As mentioned above, the behaviors of D group differ too greatly to regard it as a rock related with a Kuroko deposit positively. As C group shows behaviors similar to those of A and B groups, which are regarded as Kuroko deposit related rocks in this method, it is difficult to conclude the kind of rock of D group.

4-2-4   Cluster Analysis

For the purpose of distinguishing rocks related with Kuroko type deposits from those not related or checking for the possibility of dividing each rock group into finer groups, the cluster analysis was carried out using the results of the principal component analysis. The cluster analysis is a method to classify samples into clusters of similar geochemical characteristics in this case based on a certain criterion. The criterion used in this survey is the degree of the nearest neighbor in Euclidean distance from the origin of a six-dimensional space with the six components as axes using the first to the sixth component scores. The results of cluster analysis are shown in Fig. 4-13 in a dendrogram. By this diagram, the relationship between each sample and a cluster can be found. The alphabet before a number shows the geological unite (see previous section) from which the sample originated.

At first, 102 samples were classified into ten clusters and it was checked how the samples divided into six groups according to their collection sites were classified into the ten clusters. As a result, features were found in some clusters. The details of the clusters, which were judged to be important, are as follows.

Cluster 2: This cluster includes a group of 19 samples and all of these members are the samples related with Kuroko type deposits. Especially the seven samples of 14 samples collected in the pyroclastics of ore horizon in La America-Descubridora area are included. Therefore, it can be thought that the chemical component of rock which is closely related with Kuroko type deposits shows the average component of this cluster. Accordingly, the average chemical components of main clusters were compared (Table 4-12, Fig. 4-14).
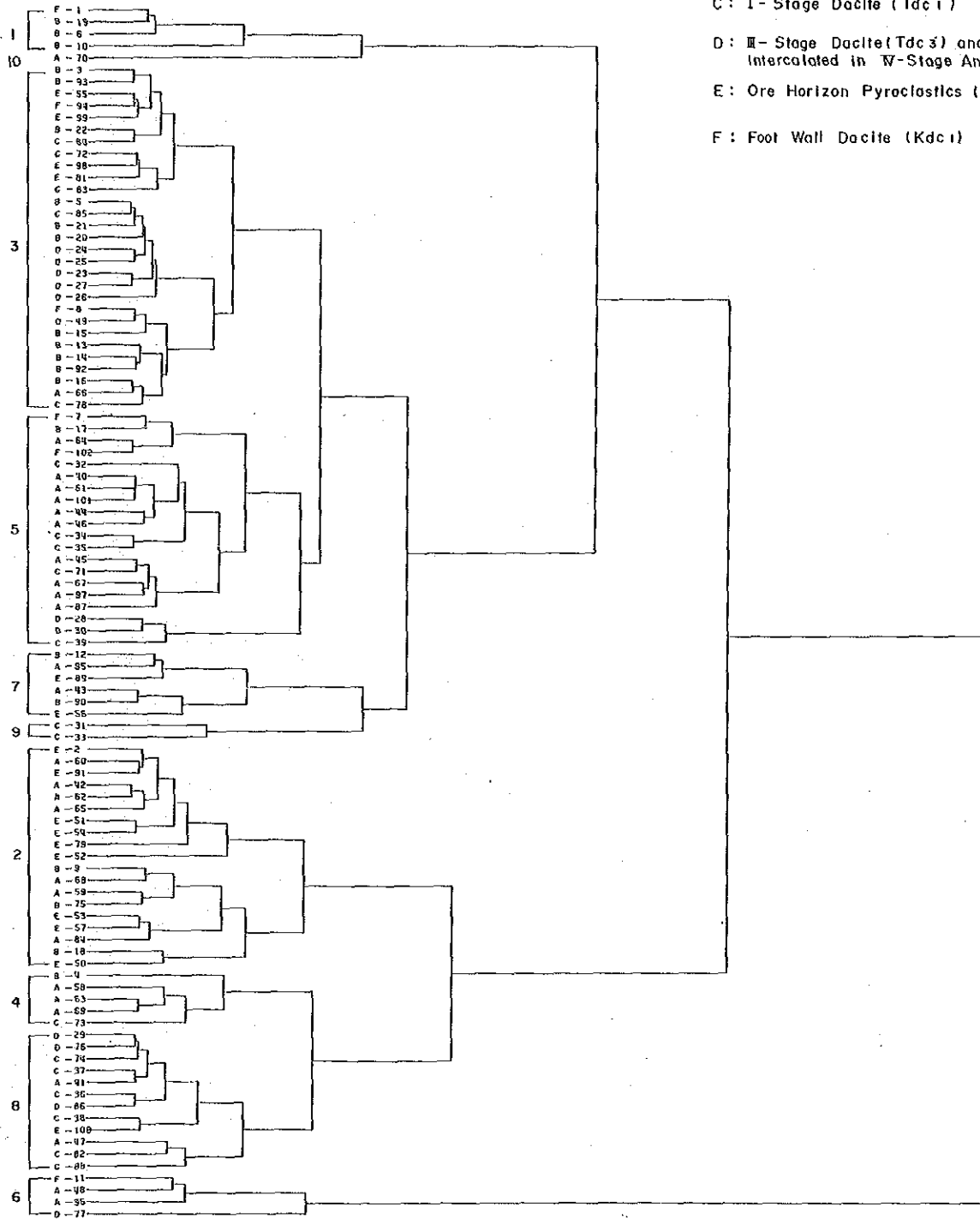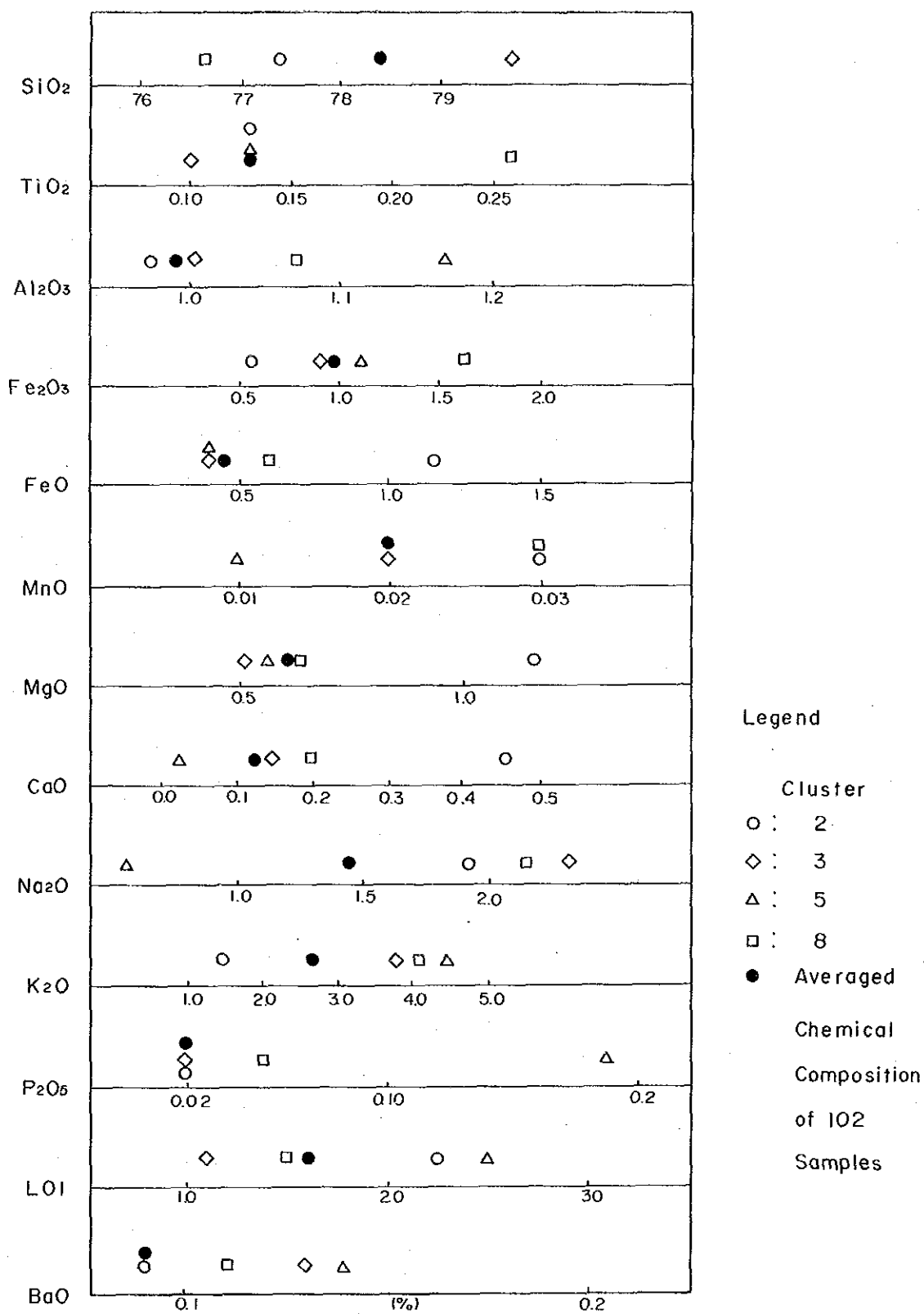
Fig.4-13 Cluster Dendrogram of Rock Samples

Fig.4-14 Comparison of Chemical Characteristcs
of Major Clusters

According to the result of comparison, this cluster has the features as follows compared with other clusters and the average of the whole rock.

(1) Relatively poor in Al_2O_3, Fe_2O_3, K_2O and BaO

(2) Relatively rich in MgO, CaO and LOI

From the fact that the samples composing this cluster is the group most closely related with Kuroko type deposits stratigraphically, increase in MgO and K_2O and decrease in CaO and Na_2O by the influence of alteration related with Kuroko type mineralization were expected, but only the behavior of MgO conformed with this tendency. In other components, the change of component percentages accompanied by the general alteration of Kuroko type deposits is not noticed. The above fact may be a feature of the alteration of the Kuroko type deposits in this survey area.

Cluster 3: This cluster includes 29 samples. The feature of this cluster is that samples related with Kuroko type deposits and which are unclear in their relation with the deposits are included together and the hanging wall dacite (Kdc_2) of La America-Descubridora area is little included. Especially, eleven of the 24 samples from the hanging wall dacite (Kdc_2) of El Rubi deposit are included. This means that, different from the former, the latter often has chemical components similar to those of the samples which are unclear in relationship with Kuroko type deposits. The features of this cluster in chemical components are as follows (Fig. 4-14).

(1) Poor in TiO_2, FeO, MgO, P_2O_5 and LOI

(2) Rich in SiO_2 and Na_2O

The feature that they are rich in SiO_2 seems to show that the samples in this cluster were subjected to silicification, but on the other hand, decrease in Na_2O, which is regarded most sensitive to hydrothermal alteration, is not noticed. It can be concluded that this cluster is characterized mainly by silicification and that it is a group of a type different from the alteration of Kuroko type deposite or which has received weak alteration only.

Cluster 5: This cluster is composed of the hanging wall dacite (Kdc_2) of La America-Descubridora area possibly related with Kuroko type deposits and dacites which are unclear in relation with deposits. On the contrary to cluster 3, few samples from the hanging wall dacite (Kdc_2) of El Rubi deposit are included. It can be said that the hanging wall dacite (Kdc_2) of La America-Descubridora area and the hanging wall dacite (Kdc_2) of El Rubi deposite are exclusive from each other in regard to the chemical components of rocks.

The features of this cluster are as follows.

(1) Poor in SiO_2, FeO, MnO, CaO and Na_2O

(2) Rich in Al_2O_3, Fe_2O_3, K_2O, P_2O_5, LOI and BaO

Among the four main clusters, this cluster is closest to the movement format of components caused by the general Kuroko type deposit alteration.

Especially, the relative decrease in Na_2O and the relative increase in K_2O are noticeable. Relative increase in BaO, the main component of barite, which is a gangue mineral of Kuroko type deposits, is also observed. However, the degree of relative increase in MgO is insufficient to immediately conclude this cluster as a cluster subjected to the Kuroko type alteration, but this cluster shows characteristics closest to the Kuroko type alteration.

Cluster 8: Nine samples of the twelve samples composing this cluster are those of unclear relation and only three samples are those related with the Kuroko type deposits (hanging wall dacite Kdc_2 and ore horizon pyroclastics Koh). This cluster can be ranked as that in which the samples of unclear relation dominate.

The features in components are as follows.

(1) Poor in SiO_2

(2) Rich in TiO_2 and Fe_2O_3

Particularly noticeable behaviors of components are not seen. The degree of alteration is judged to be weak. In addition to the above, there are clusters 1, 4, 6, 7, 9 and 10, but they are all the groups composed of a few samples and judged to give little influence upon grasping the characteristics of all the samples. Eighty percent samples are included in the above four main clusters.

Table 4-1 2   Average Chemical Composition of Principal Clusters

Composition	Cluster				Average of all rock
	2	3	5	8	
SiO_2	7 7.4 8	7 9.7 0	7 6.3 0	7 6.3 1	7 8.4 0
TiO_2	0.1 3	0.1 0	0.1 3	0.2 6	0.1 3
Al_2O_3	9.7 4	1 0.3 6	1 1.7 1	1 0.7 3	9.8 6
Fe_2O_3	0.5 5	0.8 3	1.2 2	1.7 2	0.8 4
FeO	1.3 2	0.3 2	0.3 1	0.5 2	0.4 9
MnO	0.0 3	0.0 2	0.0 1	0.0 3	0.0 2
MgO	1.2 8	0.1 3	0.2 3	0.3 4	0.3 0
CaO	0.4 5	0.1 4	0.0 2	0.2 0	0.1 2
Na_2O	1.9 3	2.3 2	0.5 6	2.1 7	1.4 4
K_2O	1.4 5	3.7 5	4.4 6	4.0 7	2.6 6
P_2O_5	0.0 2	0.0 2	0.1 9	0.0 5	0.0 2
LOI	2.2 5	1.1 1	2.4 9	1.5 1	1.6 1
BaO	0.0 9	0.1 3	0.1 4	0.1 1	0.0 9

Similarly to the principal component analysis, it was unable to define a cluster to which the foot wall dacite (Kdc_1) belongs.

Four main clusters were investigated as above. Although it is difficult to make clear distinction among them from their chemical components, the following evaluations can be given.

(1) Although a few samples from the hanging wall dacite (Kdc_2) of La America-Descubridora area are distributed into each cluster, the characteristics in components of the cluster 5 which includes the greatest number of samples from the dacite are closest to the behaviors of the chemical components shown by Kuroko type alteration among these four main clusters. Also about the state of formation of altered minerals in this hanging wall dacite (Kdc_2), the formation of sericite and chlorite over the widest area compared with other areas in this survey area was confirmed by X-ray diffractometrical study, therefore, the characteristics are closest to he Kuroko type alteration also in this point. Therefore, it can be concluded that this area is that of the strongest Kuroko type alteration.

(2) The samples from the hanging wall dacite (Kdc_2) of El Rubi deposit are also distributed to each cluster, but in the characteristics of the chemical composition of cluster 3, to which these samples concentrate most, relative decrease in Na_2O, was not noticed as mentioned above, therefore, this cluster shows different features from those of Kuroko type alteration. It can be concluded that the alteration suffered by this cluster was generally weak.

(3) Most of the ore horizon pyroclastics (Koh) of La America-Descubridora area are supposed to have received the Kuroko type alteration from their positional relation with known deposits, but the chemical component behaviors of cluster 2, to which the samples from these rocks concentrate most, seem to be considerably different in alteration type from the hanging wall dacite (Kdc_2) which covers these pyroclastics.

(4) About the samples from the areas which have no clear relation with Kuroko type deposits, there are few of these samples distributed to cluster 5 whose characteristics are most similar to those of the Kuroko type alteration. On the contrary, these samples tend to concentrate into cluster 3, which is thought to be of different type. Therefore, these dacites (Tdc_1 and Tdc_3) do not have sufficient positive evidence to judge them as rocks related with Kuroko type deposits.

CHAPTER 5   GEOPHYSICAL SURVEY

CHAPTER 5　GEOPHYSICAL SURVEY

5-1　Survey Method

5-1-1　Measuring Method

The CSAMT (Controlled-Source Audio Magnetotelluric) method determines the underground resistivity distribution by transmitting audio frequency current through the grounded dipole and measuring the electric field (E), parallel to the transmitter bipole, and the magnetic field (H), perpendicular to the electric field.

The development of a CSAMT measurement system (transmitter system and receiver system) is shown in Fig. 5-1. The transmitted current frequencies are 4096, 2048, 1024, 512, 256, 128, 64, 32, 16, 8 and 4 Hz (eleven in total).

Signals from both electrical and magnetic fields are processed by a GDP-12 receiver, which outputs the following:

(1)　Apparent resistivity　　　　　　　　　　　　　　　(ρa)

(2)　Phase difference between electric and magnetic fields　(PD)
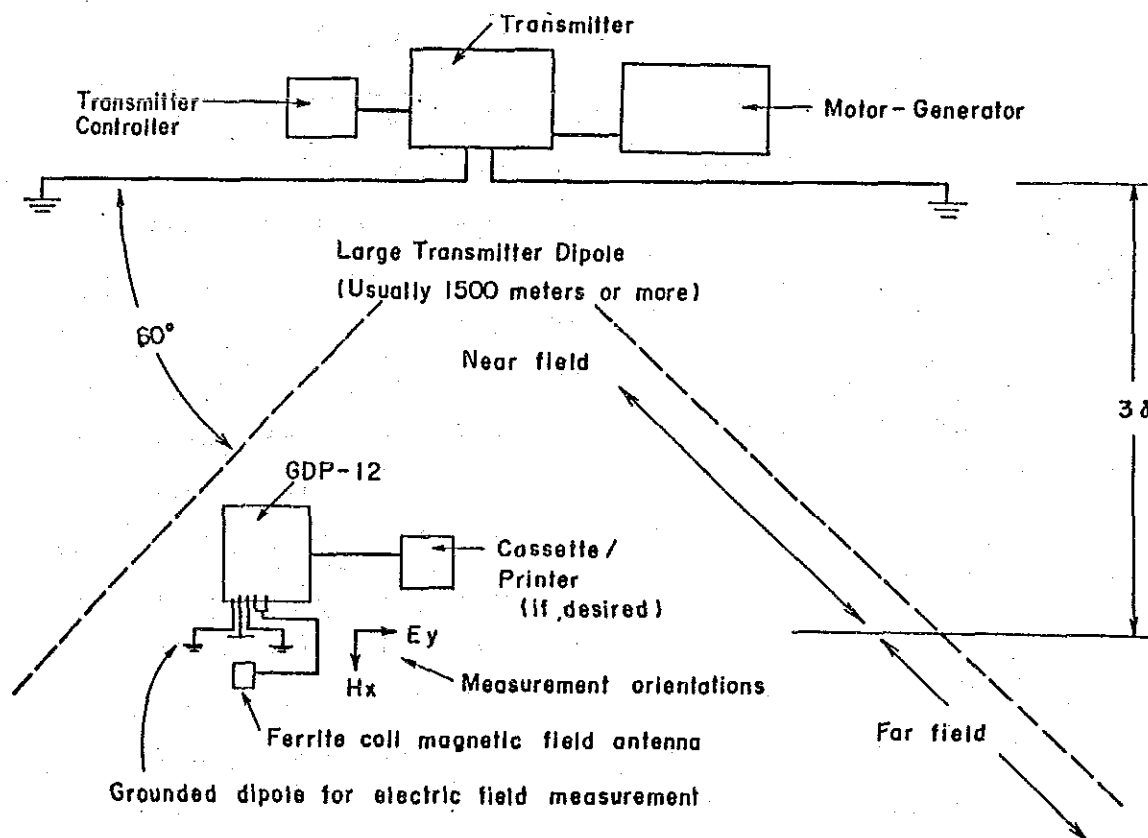
Fig. 5-1　Logistics of a CSAMT Measuring System

As shown in Fig. 5-1, the distance between the transmitter system and receiver system should be three times or more the skin depth, and then at the receiving point an assumption of plane electromagnetic waves is considered to be approximately valid (3δ: usually 5 to 10 km).

The skin depth is given by the following equation.

$$\delta = 503\sqrt{\frac{\rho}{f}} \qquad\qquad (5\text{-}1)$$

where
δ : skin depth (m)
ρ : resistivity (Ω -m)
f: frequency

Using equation (5-1), the relationship among skin depth, frequency and resistivity for a semi-infinite homogeneous medium is shown in Table 5-1. As cleary shown in table 5-1, skin depth increases with lower transmitting frequencies and higher resistivity of the medium. Consequently, the higher the resistivity is, the stronger the effect of near field becomes, thus the range of near-field data shifts from the lower frequency side to the higher frequency side.

Table 5-1 SKIN DEPTH (Meter)

Remark: Skin Depth (m) $= 503 \times \sqrt{\rho/f}$

RESISTIVITY IN OHM-METERS

Remark : Skin Depth $(m) = 503 \times \sqrt{\rho/f}$

RESISTIVITY IN OHM—METERS

f Hz	5	10	20	40	80	160	320	640	1,280	2,560	f Hz
2,048	25	35	50	70	99	141	199	281	398	562	2,048
1,024	35	50	70	99	141	199	281	398	562	795	1,024
512	50	70	99	141	199	281	398	562	795	1,124	512
256	70	99	141	199	281	398	562	795	1,124	1,591	256
128	99	141	199	281	398	562	795	1,124	1,591	2,249	128
64	141	199	281	398	562	795	1,124	1,591	2,249	3,181	64
32	199	281	398	562	795	1,124	1,591	2,249	3,181	4,499	32
16	281	398	562	795	1,124	1,591	2,249	3,181	4,499	6,362	16
8	398	562	795	1,124	1,591	2,249	3,181	4,499	6,362	8,998	8
4	562	795	1,124	1,591	2,249	3,181	4,499	6,362	8,998	12,725	4

FREQUENCY

Since this area generally has higher resistivity and there was a possibility of having much effect of near field, the current electrode system was kept more than 8 km away from the measuring area.

As shown in Fig. 5-2, Transmitter bipole No.1 and No.2 were installed in the north-eastward of the survey area.

The co-ordinates of the electrode systems and so on are shown in Table 5-2.
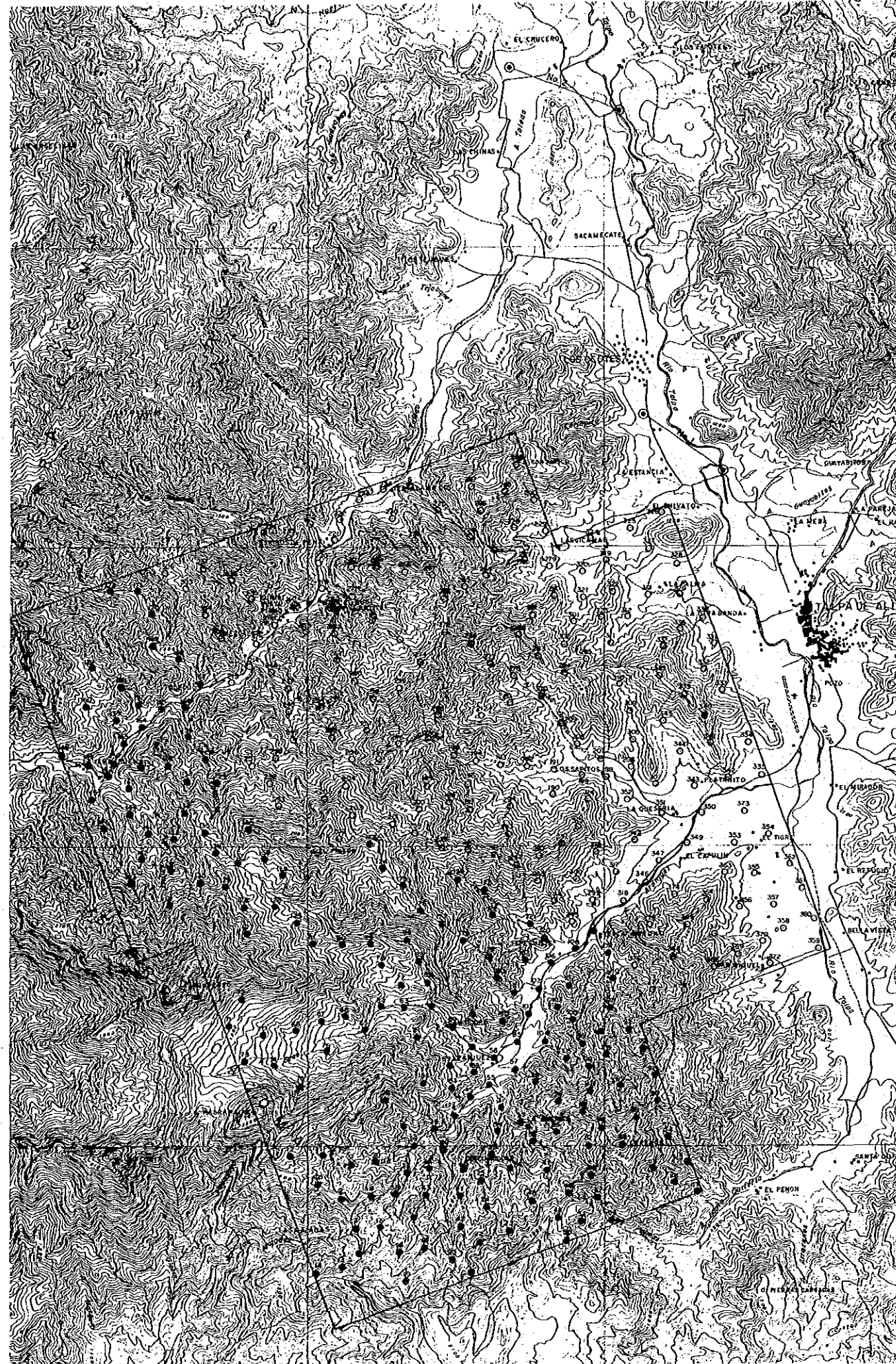
Table 5-2 Data of Transmitter Bipole

	No.1		No.2	
	X	Y	X	Y
Coordinates	10,675	32,212	8,412	37,975
	12,025	32,622	10,262	37,250
Distance between electrodes	1,670 m		1,990 m	
Direction True worth Magnetic north	N55°W N65°W		N69°W N79°W	
Corresponding survey stations	1 to 4, 7 to 187		5 to 6, 188 to 377	
Number of survey stations	185		192	

Fig. 5-2 Location Map of CSAMT Survey Stations

Many iron lods were used for current electrodes so that the total resistance of the current electrode system was less than 30Ω. In addition, to improve S/N ration, the transmitter was used in the transmitting current range 2 to 17A (mean 10 A) and in an output range of less than 9.0 kW (max.)

Measurement was made at receiving points about more than 60 m away from conductive objects such as automobiles and about more than 100 m away from power line to avoid their interference. The layout of the receiver system is shown in Fig. 5-3. To measure electric fields, three copper-copper sulphate electrodes were grounded in parallel to the transmitter bipole and 25 m away from each other. On the other hand, to measure magnetic field, a high sensivtivity ferrite coil antenna was installed more than 9 m away from, and perpendicular to, the center of the electric field dipole (potential electrodes).

Fig. 5-4 shows an example log-resistivity vs. log-frequency plot which plots frequency on X-axis and apparent resistivity on Y-axis logarithmically.

Fig.5－2

Location Map of

CSAMT Survey Stations

Transmitter

inner cable (red plug)

outer shield (black plug)

plug into the
proper channel

make sure
coil is level

CH1

CHI CH2

CH2

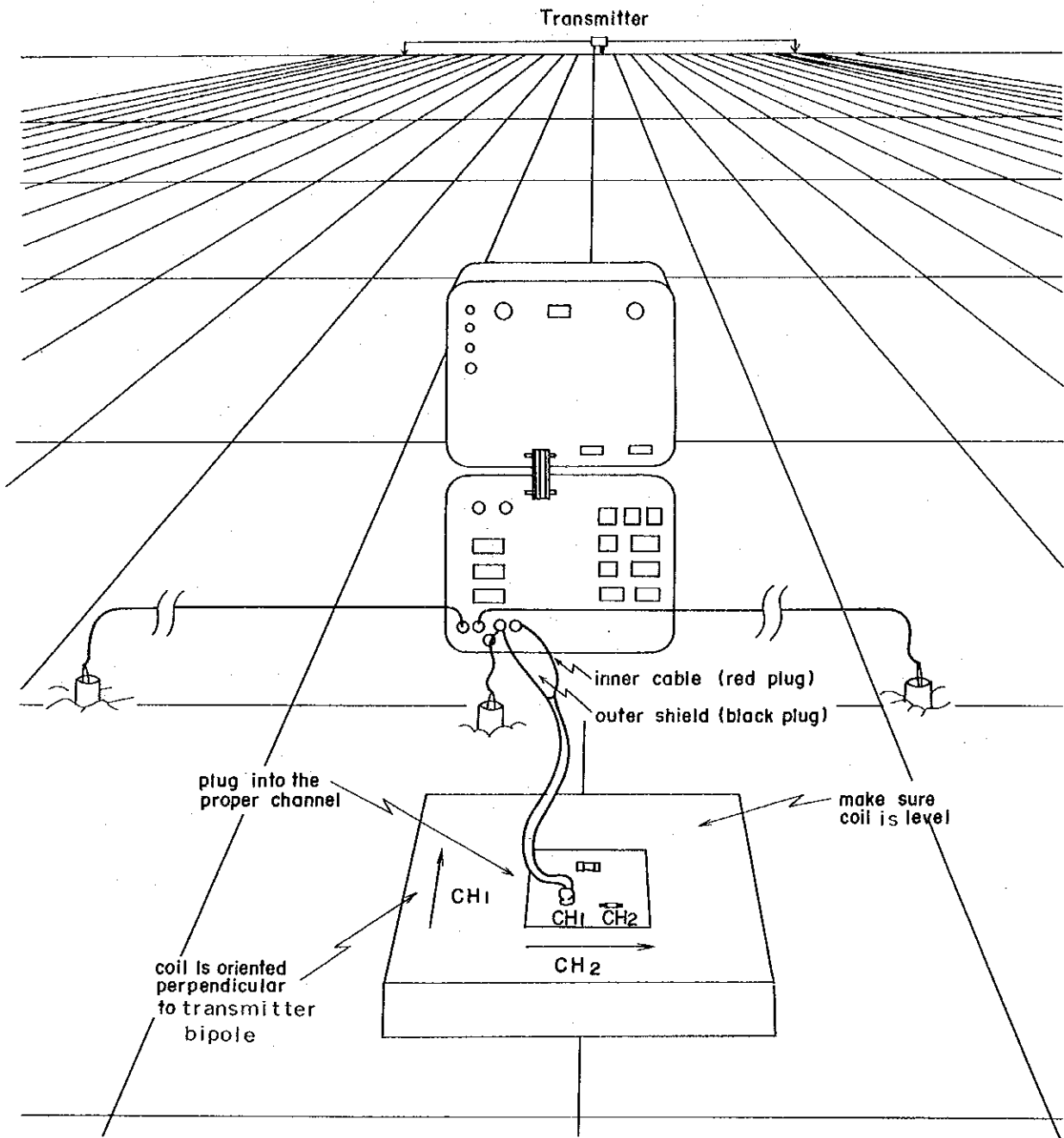coil is oriented
perpendicular
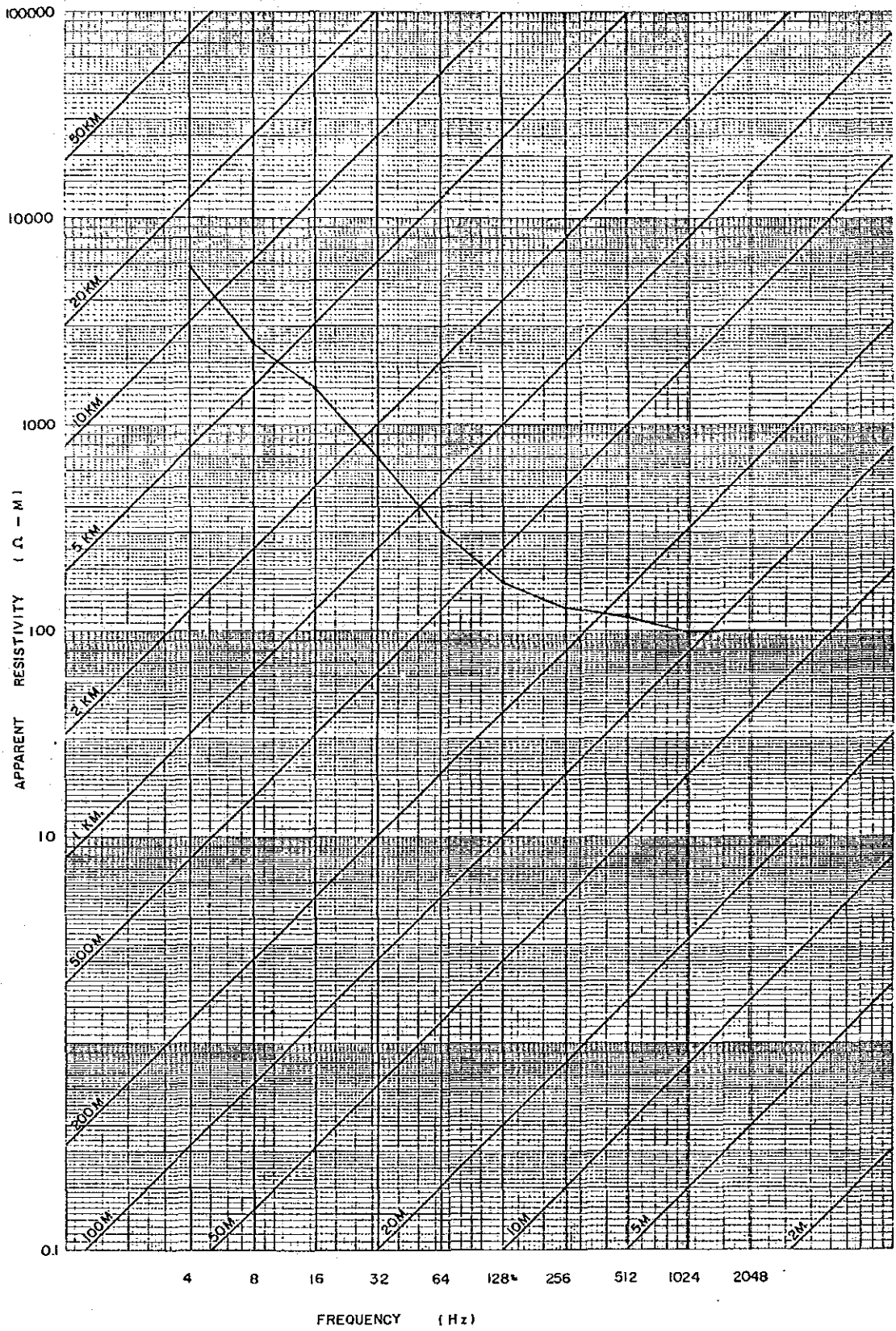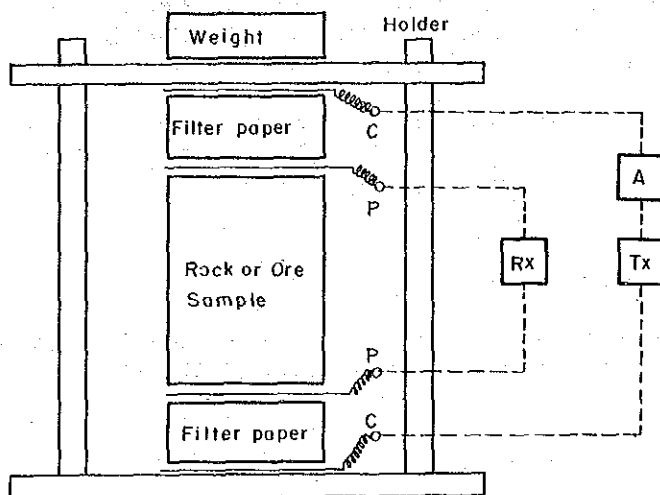to transmitter
bipole
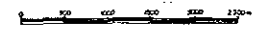
Fig. 5-3 Receiver Arrangement

Fig. 5-4 Log-Resistivity versus Log-Frequency Plot

To study the correspondence between the results of CSAMT survey and geology, 17 rock and ore samples in total, which represent geology in survey area, were collected. After all these samples had been formed into nearly rectangular prisms, their resistivity was measured in a wet state by the measurement system shown in Fig. 5-5. The values of resistivity were calculated by the following equation:

$$\rho = (V/I) \cdot (S/l) \quad \text{..........................} \quad (5-2)$$

Fig. 5-5 Block Diagram of Laboratory Measurement

where ρ: resistivity   (Ω-m)
         V: potential difference   (V)
         I: current   (A)
         S: cross-sectional area   (m^2)
         l: length   (m)

5-1-2 Instruments Used

Table 5-3 shows equipment, tools and materials which were used in measurement.

5-2 Data Processing and Analysis

5-2-1 Data Processing

The intensity and absolute phases of electric and magnetic fields are measured by the GDP-12 receiver, potential dipole and coil antenna, and then the apparaent resistivity and the phase difference between the electric and magnetic fields calculated by the microprocessor in the receiver, are displayed.

Next, all data used in measurement and calculation and the results of calculation are printed by the CAP-12 casette printer. To calculate apparent resistivity, the following Cagniard's equation (1953), being used in the ordinary MT method, is used.

$$\rho a = |Ex/Hy|^2 \, (2\pi f\mu) \, \dots\dots\dots\dots \, (5\text{-}3)$$

where   Ex: electric field (V/m), Hy = magnetic field (A·Turn/m)
  f : frequency (Hz), μ: permeability in vacuum
  $(4 \times 10^{-7} H/m)$

Hence, equation (5-3) becomes as follows:

$$\rho a = 1.267 \times 10^5/f \cdot |Ex/Hy|^2 \, \dots\dots\dots \, (5\text{-}4)$$

For measuring units, (mV/km) and (Gamma) were used for electric and magnetic fields respectively. Therefore, the following equation (5-5) was used to calculate apparent resistivity.

$$\rho a = 0.2/f \cdot |Ex/Hy|^2 \, \dots\dots\dots\dots \, (5\text{-}5)$$

In the Measured Data Lists attached to Apx. 10, mean values of E, H, RHO and PD for each frequency are listed. Since these values are used for the succeeding data processing and analysis after that, the values of apparent resistivity (RHO) in the Apx. 10 are slightly different from apparent resistivity values obtained from equation (5-5) using E and H in the Apx. 10.

With these values of RHO, a plan of apparent resistivity was drawn for each frequency, but data of 4.096 Hz was excluded from data processing and analysis after that, from the judgment that the data includes much noise.

For apparent resistivity pseudo-sections, the following four sections were selected: A-A', B-B', C-C' and D-D'. In this case they pass through major apparent resistivity anomalies and both A-A' and B-B' sections run nearly parallel to the geological structure of this area, while both C-C' and D-D' cross their direction nearly at right angles.

Table 5-3 CSAMT Survey Instruments

System	Equipment	Specification	Number
Transmitter System	Zonge, Inc. Model GGT-25 Transmitter	Output Voltage: 400 V ∿ 800 V Output Current: 0.2 A ∿ 25 A (9.0 kW)· Output Ware Form: Rectangular Output Carrent Frequency: 4 Hz ∿ 4096 Hz Weight: 113 kg	1
	Model XMT-12 Transmitter Controler	Controle Current Frequency: 4 Hz ∿ 4096 Hz Weight: 5.8 kg Power Source: 12 V Battery	1
	Model VR-1 Voltage Regurator	Weight: 3.7 kg	1
	Model ZMG-10 Engine-Generator	Maximum output Power: 10 KW Frequency: 400 Hz Rating Voltage: 115 V Engine: 23 Hp, 2 Clinder, Aircooling	1
Receiver System	Model GDP-12 Receiver	Input Signal: 2 channels AMT Receiving Frequency: 4 ∿ 4096 Hz (11 kinds) Receiving Voltage Sensitivity: 0.2 µV Weight: 15 kg Power Source: 12 V Battery	1
	Model CAP-12 Mini Casset Recorder	Weight: 6.2 kg Power Source: 12 V Battery	1
	Techtronics Model 212 Oscilloscope	Input Signal: 2 channels Power Source: 12 V Battery	1
	AMT Antena	Weight: 9.8 kg Power Source: 9 V Transister Battery	1
Electrode	Current Electrode	Iron Rod: ϕ16 mm, Length 80 cm	200
	Potential Electrode	Saturated Copper Sulphate Solution Non-Polarized Electrode	10
Wire	Fujikura Electric Kyosan Electric	VSF x 1.25 mm^2 Vinyl Wire CVV_1 x 3.5 mm^2 Vinyl Wire	1000 m 6000 m
Sample Measurement System	Chiba Electronics Institute Model CH-8108A IP Transmitter	Output Current: 1 µA ∿ 20 mA Output Wave Form: Rectangular Output Current Frequency: 0.3 Hz, 3Hz	1
	Chiba Electronics Institute Model CH-8104R IP Receiver	Receiving Voltage: 1 mV ∿ 10 V	1
	Platinum Electrode	Platinum Wire Diameter: 0.3 mm	4

In sections, apparent resistivity values on survey stations near sectional lines were plotted in a high to low frequency order to draw contour lines as drawn in the plan of apparent resistivity. Apparent resistivity values show the mean resistivity values down to skin depths. Since skin depth is a function of apparent resistivity and frequency as shown in equation (5-1). Frequency (Y-axis) does not correspond skin depth directly. These apparent resistivity pseudo-sections show the outline of vertical resistivity distribution underground.

5-2-2 Analytical Method

A simulation technique, curve-matching method, was used for analysis. In this technique, measured values are plotted on the display of a personal computer, and then a log-resistivity vs. log-frequency plot calculated for an arbitrary, resistivity multi-layered model is superposed on the display. Next, this model is corrected so that it approximates the actual CSAMT curves drawn from measured values. An example is shown in Fig. 5-6.
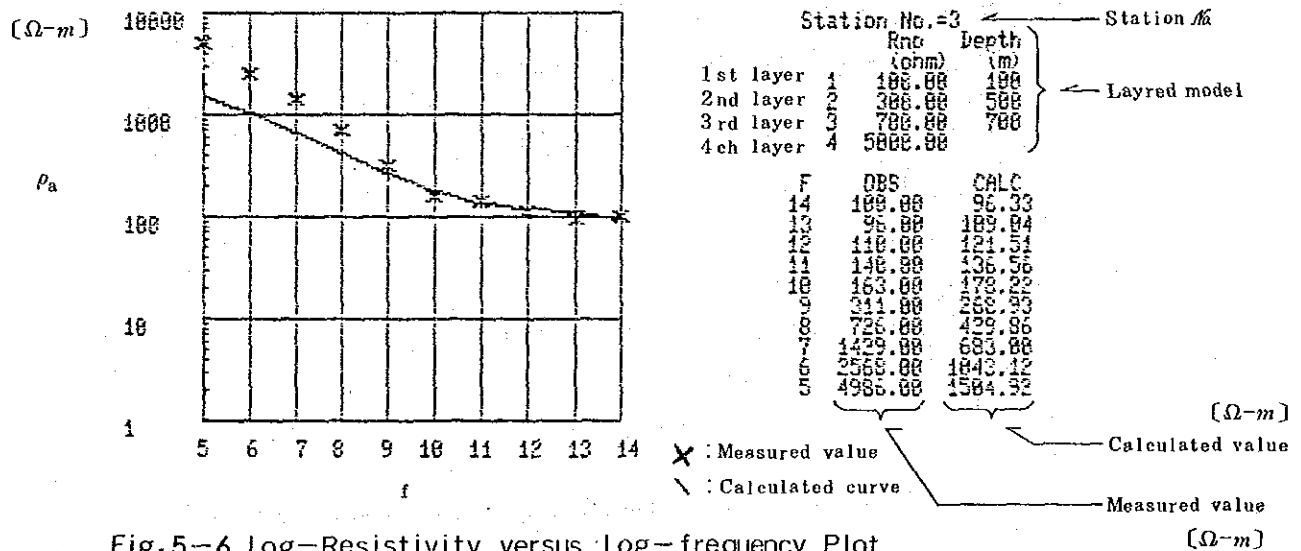
Fig.5-6 Log—Resistivity versus Log—frequency Plot
With Calculated Curve

Remark :

"f" in transversal axis is frequency №. "f" values correspond to

frequency as followings.

Frequency №	Frequency (Hz)	Frequency №	Frequency (Hz)
14	2048	9	64
13	1024	8	32
12	516	7	16
11	256	6	8
10	128	5	4

The resistivity calculation method for layered model used for the above simulation is as follows:

The surface impedance $(Z(0))$ of the $(n+1)$ the layeres, for a layered structure with resistivity values of respective layers $\rho_1, \rho_2, ..., \rho_n, \rho_{n+1}$ and depth of respective layers $Z_1, Z_2, ..., Z_n$ is shown by the following equation.

$$Z(o) = \frac{Ex}{Hy}\bigg|_{z=o} = \frac{i\omega}{\theta_0}\frac{(A_0 + B_0)}{(A_0 - B_0)} \quad .... \quad (5\text{-}6)$$

where

$$\left.\begin{array}{l} A_0 + B_0 = A_1 + B_1 \\[2mm] \theta_0 \ (A_0 - B_0) = \theta_1 \ (A_1 + B_1) \end{array}\right\} \qquad (5\text{-}7)$$

$$\left.\begin{array}{l} A_j \ \exp \ (- \theta_j \ Z_j) + B_j \ \exp \ (\theta_{j+1} \ Z_j) \\[2mm] \qquad = A_{j+1} \ \exp \ (- \theta_{j+1} \ Z_j) + B_{j+1} \ \exp \ (\theta_{j+1} \ Z_j) \\[3mm] \theta_j \ [A_j \ \exp \ (- \theta_j \ Z_j) - B_j \ \exp \ (\theta_j \ Z_j) \\[2mm] \qquad = \theta_{j+1} \ [A_{j+1} \ \exp \ (- \theta_{j+1} \ Z_j) - B_{j+1} \ \exp \ (\theta_{j+1} \ Z_j) \\[3mm] \qquad\qquad (j = 1, \ 2, \ ..... \ n) \end{array}\right\} \qquad (5\text{-}8)$$

$$\left.\begin{array}{l} A_n = \dfrac{\theta_{n+1} + \theta_n}{2\theta_n} \ \exp \ [-(\theta_{n+1} - \theta_n) \ Z_n] \\[4mm] B_n = \dfrac{\theta_{n+1} - \theta_n}{2\theta_n} \ \exp \ [-(\theta_{n+1} - \theta_n) \ Z_n] \end{array}\right\} \qquad (5\text{-}9)$$

Where the cgs·emu unit system is used and   shows the number of waves.

$$\theta_j = (\frac{4\pi i \omega}{\rho_j})^{1/2} \qquad (j = 1, \ 2, \ ..... \ n)$$

$$\omega = 2\pi f$$

On the one hand, since 1 mV/km = 1 emu, 1 Ω-m = 10^{11} emu, and 1 γ = 10^{-5} emu, the apparent resistivity equation (5-5) can be represented in the cgs·emu unit system as follows:

$$\rho a = \frac{2}{f} \left| Z(0) \right|^2 \ (\text{emu}) \qquad .... \ (5\text{-}10)$$

Accordingly, apparent resistivity (ρa) can be determined from equations (5-6) to (5-10), and the equation for calculating ρa in Ω-m unit becomes as follows:

$$\rho a = 2/f \cdot \left| Z(0) \right|^2 / 10^{11} \quad (\Omega\text{-m}) \ .... \ (5\text{-}11)$$

In consideration of the resistivity layered model, results obtained from Bostic Inversion were referred to.

The ρa-f curves frequently show three zones, far-field (F), transition-zone (T) and near-field (N) as seen in Fig. 5-7. Near-field data shows a straight line with approximately -45° gradient on the low frequency side of Log-Resistivity versus Log-Frequency Plot.
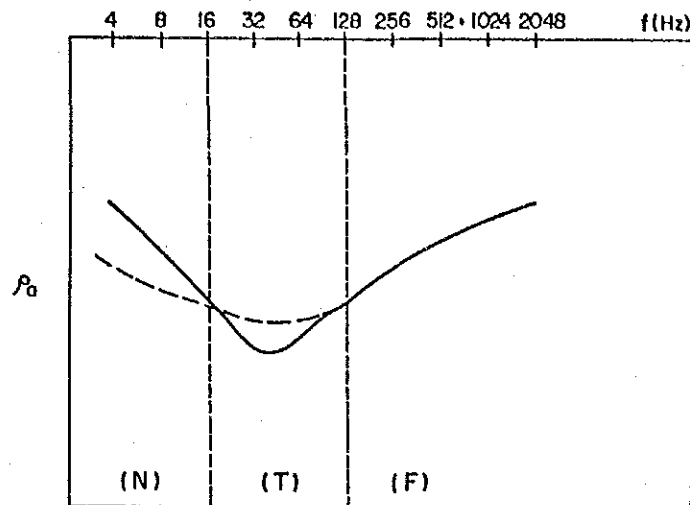

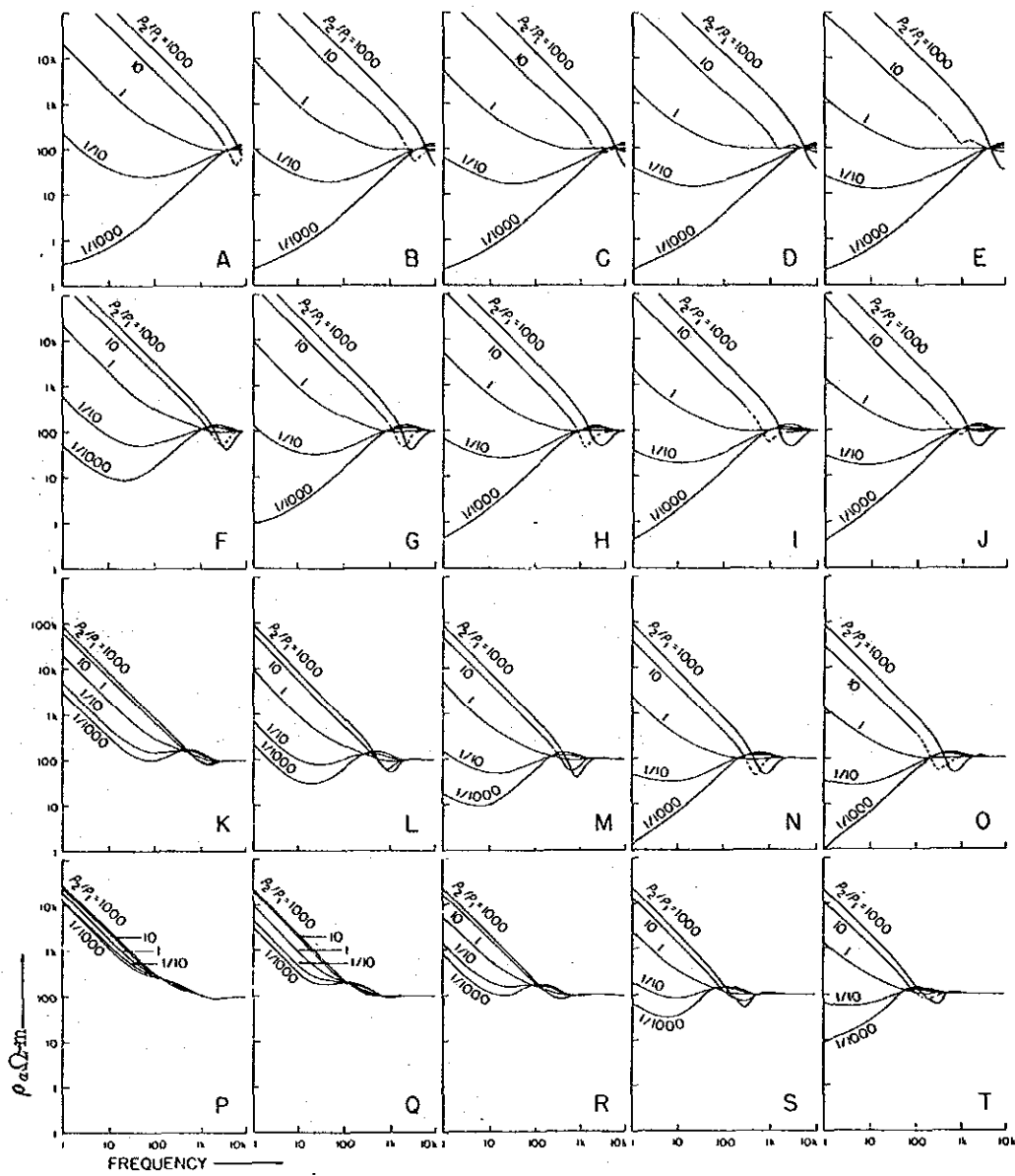Fig. 5-7 Typical CSAMT Log-Resistivity versus Log-Frequency Plot

(F): far-field data
(T): transition-zone
(N): near-field data

The dashed line gives the Calculated Curve

(Zonge, Inc, Interpretation Guide for CSAMT Data, 1982)

For reference the features of ρa-f curve of the two-layered structure model are shown in Fig. 5-8. In the figure, the curves show transition-zones as well as near-field zones when the second layer is of high resistivity.

Thus, in this analysis, a model having high resistivity at the lowest layer was assumed for simulation of data including near-field and transition zones. In addition, curve matching was carried out so that calculated curves passed the upper part of transition zones and lower part of near-field zones as shown in Fig. 5-7.

Fig. 5-8 Representative Families of Curves for Various Depth to the Bottom of the First Layer and Various Ranges

D	R = 5 0 0 m	7 5 0 m	1, 0 0 0 m	1, 5 0 0 m	2, 0 0 0 m
5 0 m	A	B	C	D	E
1 2 5 m	F	G	H	I	J
2 5 0 m	K	L	M	N	O
5 0 0 m	P	Q	R	S	T

ρ_1, ρ_2: resistivity of the first and second layers respectively.
$\rho_1 = 100$ Ω-m
R: distance between Tx bipole and receiver point
D: thicikness of the first layer

(Goldstein & Strangway, 1975)

Various plans of resistivity structure was produced based on the layered resistivity model for each survey station obtained from simulation. These plans show the underground resistivity structure at the depths of 100 m, 200 m, 400 m and 800 m below the surface of each survey station.

In the structural resistivity section, the same cross-sectional lines as in an apparent resistivity section are used, and the layered resistivity model obtained from simulation analysis is plotted with the depths from the ground surface. In addition, it shows the underground resistivity structure expressed by connecting layered models, each having similar values of resistivity.

For each section such as A-A', B-B', C-C' and D-D', the apparent resistivity, resistivity structure and geological sections were arranged respectively.

5-3 Survey Results and Interpretation

5-3-1 Survey Results

The measured data lists and the table of comparison between resistivity anomaly and geology are shown in Apx. 10 and 11 respectively.

(1) Plans of Apparent Resistivity

Plans of apparent resistivity are shown in Pls. 9 to 19 (1/25,000) and Figs. 5-9 to 5-12, and a geological map of geophysical survey area in Fig. 5-13. Since Fig. 5-9 (2,048 Hz) is considered to be suited to obtain information of upper layers, apparent resistivity anomaly zones are shown in the figure by symbols. In other words, apparent resistivity low anomaly zones are shown by L1 to L22, while apparent resistivity high anomaly zones by H1 to H15. The apparent resistivity anormaly is classified into the following zones:

|	
Apparent resistivity low anomaly zone (hereinafter called low anomaly zone - LAZ)	Less than 200 Ω -m
Apparent resistivity medium anomaly zone (MAZ)	200 to 2,000 Ω -m
Apparent resistivity high anomaly zone (HAZ)	More than 2,000 Ω -m

The distribution of apparent resistivity is characterized as follows:

. LAZs are distributed in the east to southwest of the area and around La America - Descubridora tunnels and EL Rubi tunnel.

. HAZs are distributed in the north to northwest of the area.

. In the central part of the area, MAZs or HAZs are mainly distributed, LAZs being of small scale.

The survey area is divided into the following four parts: east, south, central and north. Features of anomaly zones in each parts are described below respectively.

. In the east part of the area, many LAZs such as L7 to L12, L20 and L21 are distributed. They decline with lower frequency and are distributed in the low and flat ground of the topography. These LAZs are found on the Quaternary (Q) and the Tertiary sandstone formation (Tss$_1$) distributed in the southern highlands.

. In the south part of the area, L1 to L6 (LAZs) are distributed as if they surrounded H2 (MAZ/HAZ). While L2 to L6 shift to high resistivity gradually with lower frequency, L1 tends to be distributed in a wide range. H2 is distributed nearly from east to west, and in the depth it is further separated into two parts. One runs from east to west, the other surrounded L5. L2 (MAZ or HAZ), is distributed harmoniously with the hanging wall dacite (Kdc$_2$) and tuff (Koh), and La America and Descubriaora, known deposits, are located in the north and west edges of L2 respectively. L1, L4 and L5 and distributed in the direction of northeast like a belt, along the west to north sides of H2. Both L2 and L3 are distributed in the south and east edges of H2 respectively and in their ground surface sandstone formation (Tss$_1$) are distributed.

. There is no LAZ of large-scale in the central part of the area. Both L15 and L22 (LAZs) are of very small scale. L13 (LAZ) is located in the border of sandstone formation (Tss$_1$) and andesite intrusive (Ad$_1$) that are distributed in the Cerro El Pintor mountain mass. L15 (LAZ) is of small-scale but combines with L19 (LAZ) in the depth.

. In the northern part of the area, H15 (HAZ) on the north side of the El Rubi tunnel and H12 (HAZ) in the vicinity of Toledo are conspicuous. H15 (HAZ) shows the highest apparent resistivity within the survey area, and combines H11 to H14 (HAZs) in the depth. H15 corresponds suitably with granophyre (Gph) distributed in the ground surface. The hanging wall dacite (Kdc$_2$) and foot wall dacite (Kdc$_1$) of the El Rubi deposit are distributed on the south edge of H15. Each of L16 to L19 (LAZs) are found on the edge of H15 (HAZ). L16 shows a medium resistivity value of under 500 Ω-m on the plan of apparent resistivity for 2,048 Hz, but it is found as a small-scale LAZ with a resistivity value of under 200 Ω-m on the plan of apparent resistivity for 512 Hz. L18 (LAZ) is an anomaly in the shallow which extends from the Ocotitlan tunnel and its vicinity to the southwest. L19 (LAZ) extends down to the depth where it is connected to L15 (LAZ) like a belt.
· L19 and the andesite intrusive (Ad$_1$) have the same direction.

Observing plans of apparent resistivity in terms of distribution scales, extension down to the depth and geology, noteworthy LAZs from the viewpoint of mineral exploration are probably L1, L2, L4 and L5 in the vicinity of the La America – Descubridora deposit, and L16 and L18 in the vicinity of the El Rubi deposit.
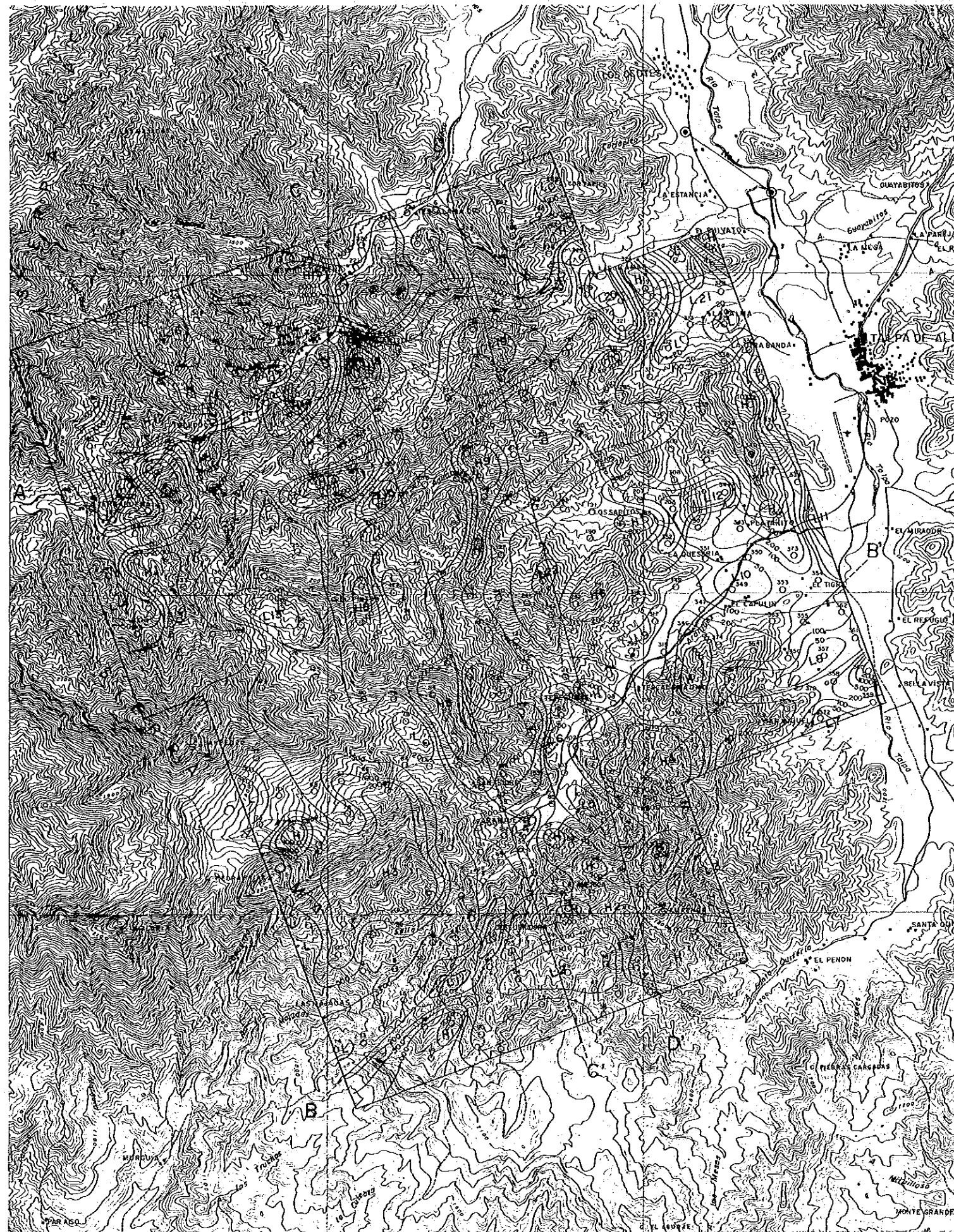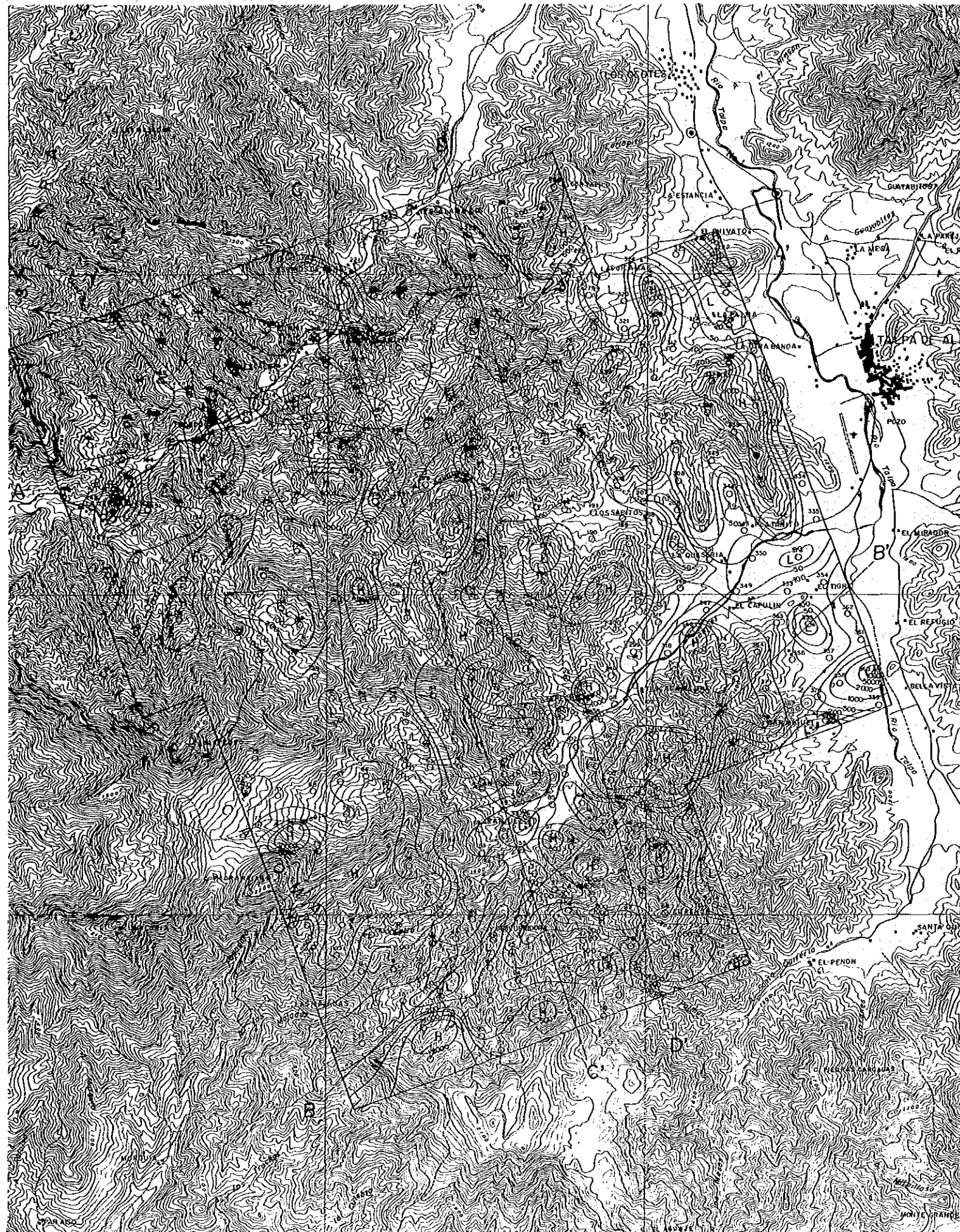
LEGEND

|	
$\overset{377}{\bigcirc}$	Station Point, No.
⊙——⊙	Transmitter Bipole
⌒-100-	Contour of Apparent Resistivity (Ω-m)
L3	Low Resistivity Anomaly, No.
H4	High Resistivity Anomaly, No.

Fig.5−9

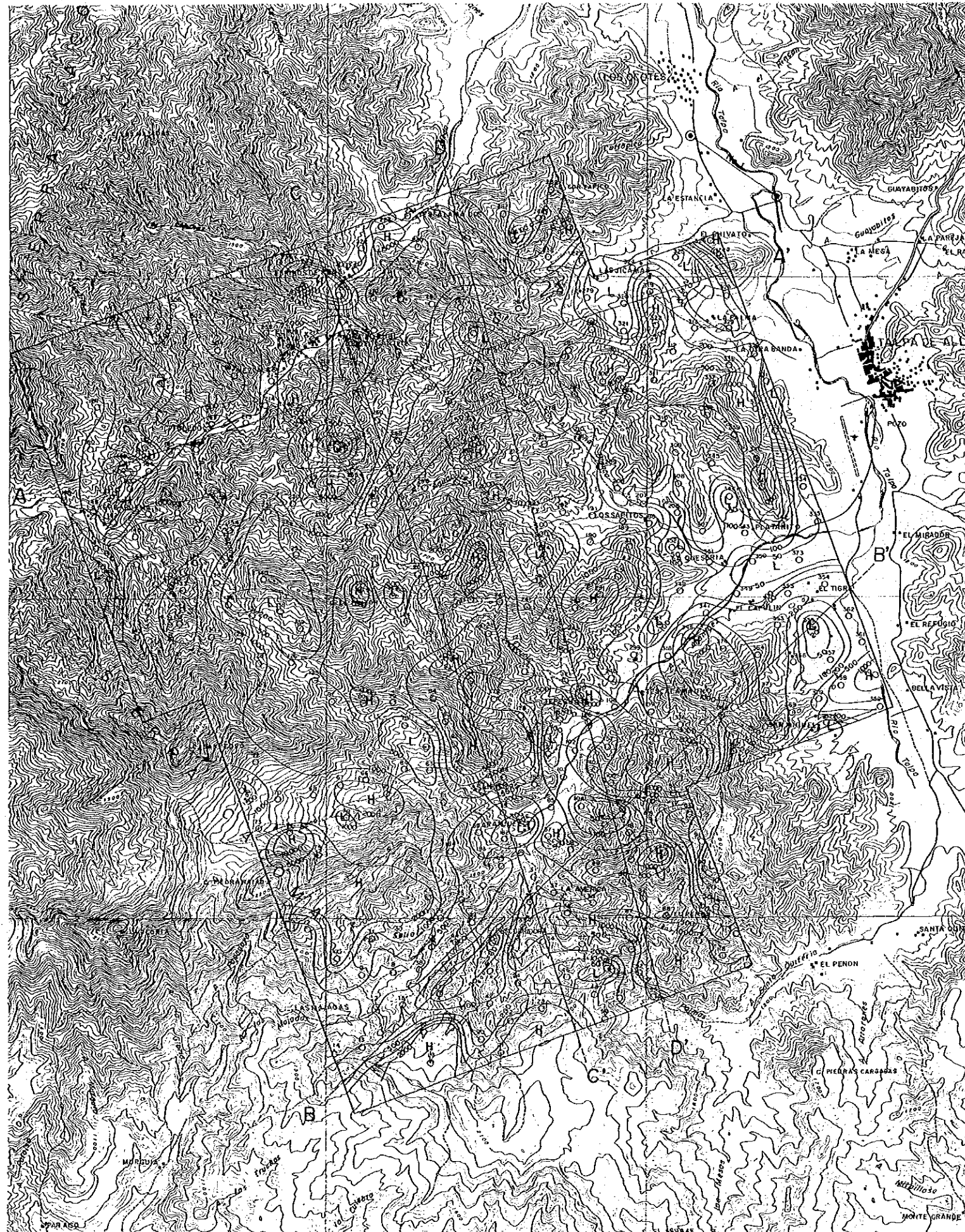Plan of Apparent Resistivity

(2048Hz)

LEGEND

⊙ Station Point, No.
377

⊙——⊙ Transmitter Bipole

◯100◯ Contour of Apparent Resistivity (Ω-m)

Fig. 5—10

Plan of Apparent Resistivity

(1024 Hz)

Fig. 5-11

Plan of Apparent Resistivity

(512Hz)